February 1999

Characterisation of the Strain Rate and Temperature Dependence of the Properties of Plastics for the Prediction of Impact Performance

B E Read, G D Dean and B C Duncan
Centre for Materials Measurement & Technology
National Physical Laboratory, Teddington
Middlesex TW11 0LW, UK

SUMMARY

Tensile and shear stress-strain data have been obtained over wide ranges of strain rate and at different temperatures for polycarbonate, a propylene-ethylene copolymer and an acrylonitrile-butadiene-styrene (ABS) copolymer. The results are intended for use with elastic-plastic models in finite element calculations of the impact behaviour of components. The tensile measurements were made using a combination of electromechanical, servohydraulic and impact testing machines which provided stress-strain curves at strain rates between 10^{-4} and 100 s^{-1} and temperatures of -40, 0, 23 and 50 °C. The shear tests were carried out at 0, 23 and 50 °C and gave curves of effective stress ($\bar{\sigma}$) versus effective strain ($\bar{\varepsilon}$) at effective strain rates between 10^{-4} and 10^{-1} s^{-1} which corresponded to strain rates employed in the tensile studies.

Young's moduli (E) and Poisson's ratios (ν_e) were evaluated from tensile data in the strain range 0.0005-0.0025. Increases in the value of E with increasing strain rate and decreasing temperature are most marked for the propylene-ethylene copolymer. These results, and associated variations of ν_e, are attributed to the α and β relaxation processes which are operative in this material over the ranges of strain rate and temperature investigated.

For each material, the peak or plateau yield stress on the stress-strain curve increases with increasing strain rate and decreasing temperature. The tensile stress-strain curves for the propylene-ethylene copolymer and for ABS also exhibit progressive shape changes with varying rate and temperature, and differences are observed between these curves and the $\bar{\sigma}$ versus $\bar{\varepsilon}$ curves from the shear data at corresponding effective strain rates and temperatures. These differences increase with increasing rate and decreasing temperature and are attributed to increased contributions from cavitation to the yielding under tension.

The dependence of peak or plateau yield stresses on strain rate and temperature has been successfully analysed using a generalisation of Eyring's model. This allows for contributions to the yield stress from α and β relaxation processes and enables accurate predictions to be made of the yield behaviour at impact rates by means of extrapolation or rate-temperature equivalence.

ISSN 1361-4061

National Physical Laboratory
Teddington, Middlesex, UK, TW11 0LW

Approved on behalf of Managing Director, NPL, by Dr C Lea,
Head, Centre for Materials Measurement and Technology

CONTENTS

1	**INTRODUCTION**		1
2	**OUTLINE OF ELASTIC-PLASTIC MODELS**		1
	2.1	SHEAR YIELDING	1
	2.2	CAVITATION	2
3	**DETERMINATION OF PARAMETERS**		3
	3.1	MODULUS AND POISSON'S RATIO	3
	3.2	STRAIN HARDENING FUNCTIONS	3
		3.2.1 Variation of $\bar{\sigma}$ with $\bar{\varepsilon}_p$	3
		3.2.2 Variation of $\bar{\sigma}^c$ with $\bar{\varepsilon}_p^c$	4
	3.3	SHEAR YIELD PARAMETER λ	4
4	**A MODEL FOR THE STRAIN RATE AND TEMPERATURE DEPENDENCE OF YIELD STRESS**		4
5	**EXPERIMENTAL**		5
	5.1	MATERIALS	5
	5.2	MEASUREMENTS AT LOW STRAIN RATES (10^{-5} - 10^{-1} s^{-1})	6
		5.2.1 Tensile Measurements	6
		5.2.2 Shear Measurements	6
	5.3	TENSILE MEASUREMENTS AT HIGH STRAIN RATES (10^{-2} - 100 s^{-1})	7
		5.3.1 Measurements with a Servohydraulic Machine	7
		5.3.2 Measurements with Impact Apparatus	7
		5.3.3 Identification of Data Sets and Corrections to Strain Values	7
		5.3.4 Estimation of Transverse Strains and True Stresses	8
6	**RESULTS AND DISCUSSION**		8
	6.1	ELASTIC MODULI AND POISSON'S RATIOS	8
	6.2	TENSILE STRESS-STRAIN CURVES	9
	6.3	EFFECTIVE STRESS-STRAIN CURVES FROM SHEAR DATA. COMPARISON WITH TENSILE CURVES	10
	6.4	DEPENDENCE OF PEAK OR PLATEAU STRESSES ON STRAIN RATE AND TEMPERATURE	10
	6.5	STRAIN RATE AND TEMPERATURE DEPENDENCE OF λ AND tan ψ	12
7	**CONCLUSIONS**		13
8	**ACKNOWLEDGEMENTS**		13
9	**REFERENCES**		14
FIGURE CAPTIONS			15

1 INTRODUCTION

In a previous report[1], details were presented of an elastic-plastic model for the shear yielding and non-linear, stress-strain behaviour of polymeric materials. Such models are currently employed in finite element (FE) calculations of the complex patterns of deformation and stress distributions in plastic components under load. Values of the parameters appearing in these models were derived using a combination of uniaxial tension, shear and uniaxial compression tests, and were presented for four different plastics at 23 °C and at a specified strain rate for each material. The materials studied were polycarbonate, polypropylene, a propylene-ethylene copolymer and an acrylonitrile-butadine-styrene copolymer (ABS).

For polycarbonate and polypropylene the results were consistent with a pressure-modified von Mises yield criterion, suggesting that for all stress states so far investigated (for tensile strains up to 0.3) yielding predominantly involved a shear mechanism. For the propylene-ethylene copolymer and ABS, each of which contains a dispersed rubbery phase, the shear and compressive data were similarly consistent with a pressure-modified von Mises criterion and hence with a shear yield process. However, a different yield mechanism under tension was reflected by a difference in shape between the tensile stress-strain curves and the corresponding shear and compressive curves. As this result was accompanied by stress whitening and a pronounced volume increase (decrease in Poisson's ratio) it was attributed to the onset of cavitation in these materials. This could involve the generation of voids in the rubber particles and/or crazing of the glassy matrix. Assuming that the cavitation is dominated by crazing, an additional yield criterion was proposed for those stress states having a dilatational component sufficient to initiate the cavities.

Recognising the possible involvement of two yield mechanisms, the purpose of this report is to present and discuss the strain rate and temperature dependence of relevant data obtained for polycarbonate, the propylene-ethylene copolymer and ABS. Since there is particular interest in the response of components to impact loads, emphasis is given to methods for predicting data up to high strain rates through interpolation, extrapolation or rate-temperature equivalence.

2 OUTLINE OF ELASTIC-PLASTIC MODELS

2.1 SHEAR YIELDING

With the elastic-plastic models, the linear region usually observed in a tensile stress-strain curve at low strains ($\leq$0.01) is characterised by a value for Young's modulus E and Poisson's ratio ν_e. The onset of non-linearity in the curve is then attributed to plastic deformation, and subsequent increases in stress (now regarded as the yield stress) are associated with strain hardening. For multiaxial stress states, shear yielding is assumed to occur when the second invariant of the deviatoric stress tensor

$$J_{2D} = \frac{1}{6}\left[(\sigma_1 - \sigma_2)^2 + (\sigma_2 - \sigma_3)^2 + (\sigma_3 - \sigma_1)^2\right] \qquad (1)$$

attains a critical value. Here the principal stress components σ_n (n = 1,2,3) are true stresses (referred to the strained cross-sectional area). Shear yielding in plastics is known to further depend on the hydrostatic component of stress or stress invariant

$$J_1 = \sigma_1 + \sigma_2 + \sigma_3 \tag{2}$$

and it is often assumed that yielding will occur at an effective stress $\bar{\sigma}$ given by

$$\bar{\sigma} = \sigma_T = AJ_{2D}^{1/2} + BJ_1 \tag{3}$$

where σ_T is the (true) yield stress under uniaxial tension and

$$A = \frac{\sqrt{3}(\lambda + 1)}{2\lambda}; \quad B = \frac{(\lambda - 1)}{2\lambda} \tag{3a}$$

The parameter λ, which provides a measure of the sensitivity of yielding to the hydrostatic component of stress, equals σ_C/σ_T where σ_C is the yield stress under uniaxial compression associated with the same effective plastic strain (see below) as σ_T.

With the elastic-plastic models, all normal strains ε are defined as true (natural) strains $\varepsilon = \ln(1+\varepsilon')$ where ε' is the corresponding engineering strain. In the non-linear region of a tensile stress-strain curve the strain ε_T is regarded as the sum of an elastic component $\varepsilon_e = \ln(1+(\sigma_T/E)) \approx \sigma_T/E$ and a plastic component ε_{pT} that is non-recoverable. For multiaxial loading, an effective plastic strain $\bar{\varepsilon}_p$ is equated to ε_{pT} and defined in the form of equation (3) in terms of the principal components ε_{pn} (n = 1,2,3) of plastic strain[1]. We may thus define an effective strain by

$$\bar{\varepsilon} = \varepsilon_T = \varepsilon_e + \bar{\varepsilon}_p \tag{4}$$

with $\varepsilon_e = \ln(1+(\bar{\sigma}/E)) \approx \bar{\sigma}/E$.

The effects of strain hardening may now be specified as the dependence of $\bar{\sigma}$ on $\bar{\varepsilon}_p$. From measurements of ν_p, the plastic component of Poisson's ratio[1], values can also be determined for the flow parameter

$$\tan\psi = \frac{3(1-2\nu_p)}{2(1+\nu_p)} \tag{5}$$

which provides a measure of volume change during the predominantly shear yielding and is required for relating increments of plastic strain to the components of stress. For yielding at constant volume it follows that $\nu_p = 0.5$ and thus $\psi = 0$. If the yielding is insensitive to the hydrostatic stress component then $\sigma_C = \sigma_T$, $\lambda = 1$ and we have from (3) the von Mises criterion

$$\sigma_T = \sqrt{3}J_{2D}^{1/2} \tag{6}$$

2.2 CAVITATION

Yield processes in certain plastics may involve the onset of cavitation and substantial volume increases if the hydrostatic component of stress is sufficiently large. Such processes are prominent, for example, in rubber-toughened plastics under tension and may be associated with multiple crazing in the matrix polymer and/or with cavitation of the

dispersed rubber particles. Assuming that matrix crazing is the dominant mechanism, we have proposed that cavities are initiated at a critical effective stress $\bar{\sigma}^c$ that is numerically equal to the uniaxial tensile stress σ_T and related to J_1 and $J_{2D}^{1/2}$ by

$$\bar{\sigma}^c = \sigma_T = CJ_{2D}^{1/2} - D/J_1 \qquad (7)$$

The parameters C and D may each be related to a single material parameter $\eta=\sigma_T^*/\sigma_T$ where σ_T^* is the yield stress in an equibiaxial tension test or to a parameter $\chi = \sigma_B/\sigma_T$ where σ_B is the yield stress determined in a butt tension test[1] for which an equitriaxial stress state exists during yield. The different yield stresses σ_T, σ_T^* and σ_B each refer to the same effective plastic strain $\bar{\varepsilon}_p^c$, relationships for which have been derived[1]. Assuming that shear yielding becomes negligible during the growth of crazes, the strain hardening or softening associated with this growth can be represented by the dependence of $\sigma_T (=\bar{\sigma}^c)$ on $\varepsilon_{pT} (=\bar{\varepsilon}_p^c)$.

3 DETERMINATION OF PARAMETERS

This section summarises methods for obtaining the model parameters required in calculations for different stress states and different polymeric materials. Since values for most of the parameters will depend on strain rate and temperature, they should be determined over ranges of these variables appropriate to a given application.

3.1 MODULUS AND POISSON'S RATIO

Values of E and ν_e are derived from measurements of stress, strain and transverse strain in tensile tests at low strains where the stress-strain plot is essentially linear[1].

3.2 STRAIN HARDENING FUNCTIONS

3.2.1 Variation of $\bar{\sigma}$ with $\bar{\varepsilon}_p$

If yielding under uniaxial tension involves shear deformation with no cavitation (as observed for polycarbonate) then $\bar{\sigma}$ and $\bar{\varepsilon}_p$ can be identified with σ_T and ε_{pT}, respectively, and thus determined from tensile tests[1]. If, however, cavitation occurs under uniaxial tension (as found for the propylene-ethylene copolymer and ABS) then an alternative test method such as shear or uniaxial compression must be employed. These methods require a knowledge of the value of λ (see Section 3.3 below) and are based on the relationships[1]

$$\bar{\sigma} = \frac{\sqrt{3}(\lambda+1)}{2\lambda}\sigma_S = \frac{\sigma_C}{\lambda} \qquad (8)$$

$$\bar{\varepsilon}_p = \frac{\sqrt{3}(\lambda+1)}{4\lambda(1+\nu_p)}\gamma_p = \frac{\varepsilon_{pC}}{\lambda}$$

where σ_S and γ_p are the shear yield stress and shear plastic strain, respectively, and ε_{pC} is the plastic strain under uniaxial compression.

3.2.2 Variation of $\bar{\sigma}^c$ with $\bar{\varepsilon}_p^c$

If cavitation occurs under uniaxial tension, and is associated with the initiation and growth of crazes, then values of $\bar{\sigma}^c$ and $\bar{\varepsilon}_p^c$ may be identified with the measured σ_T and ε_{pT}. This assumes that shear yielding becomes negligible once the crazes have initiated.

3.3 SHEAR YIELD PARAMETER λ

The determination of a value for λ requires measurements under two different stress states each of which produce shear yielding with no cavitation. If cavitation does not occur under uniaxial tension then λ may be derived either from tensile and compressive data or from tensile and shear data, using[1]

$$\lambda = \frac{\sigma_C}{\sigma_T} = \frac{\sqrt{3}(\sigma_S / \sigma_T)}{2 - \sqrt{3}(\sigma_S / \sigma_T)} \tag{10}$$

If cavitation does occur under tension, then λ may be evaluated from shear and compression data. This method is based on the relation

$$\lambda = \frac{2 - \sqrt{3}(\sigma_S / \sigma_C)}{\sqrt{3}(\sigma_S / \sigma_C)} \tag{11}$$

which follows from equation (8). It should be emphasised that the stresses σ_T, σ_C and σ_S in (10) and (11) each refer to the same effective plastic strain and effective plastic strain rate. Details of methods for deriving these stresses are given in a previous report[1].

4 A MODEL FOR THE STRAIN RATE AND TEMPERATURE DEPENDENCE OF YIELD STRESS

Variations in the yield stress with strain rate and temperature may be described for polymers on the basis of a model introduced by Eyring and coworkers[2]. The model considers that an increase in stress increases the net rate of molecular rearrangements in the material, and that a peak or plateau in the stress-strain curve is obtained when the strain rate produced by these rearrangements equals the applied strain rate. The molecular motions are represented by thermally activated transitions across a potential energy barrier separating two minima (Fig 1). It is then proposed that the levels of the minima are respectively raised and lowered by an amount σv where σ is the applied stress and v the volume of the moving molecular segments (the so-called activation volume). The barrier height, or activation energy, Q is thus effectively lowered and raised for transitions in the forward and reverse directions respectively. The strain rate $\dot{\varepsilon}$ is then assumed to be proportional to the net molecular flow rate in the forward direction

$$\dot{\varepsilon} = kv_o \left[\exp\left(-\frac{(Q - \sigma v)}{RT} \right) - \exp\left(-\frac{(Q + \sigma v)}{RT} \right) \right]$$

$$= \dot{\varepsilon}_o \exp\left(-\frac{Q}{RT}\right)\sinh\left(\frac{\sigma v}{RT}\right) \qquad (12a)$$

$$= \frac{\dot{\varepsilon}_o}{}\exp\left(-\frac{(Q-\sigma v)}{}\right) \quad \text{for}\frac{\sigma v}{} \qquad (12b)$$

where T is the absolute temperature, ν_o involves the molecular vibration frequency and the entropy contribution to the free energy, k is a constant and $\dot{\varepsilon}_o = 2k\nu_o$. For large stress it follows from (12b) that

$$\frac{\sigma_y}{T} = A\left[\ln 2C\dot{\varepsilon}_y + (Q/RT)\right] \qquad (13)$$

where A = R/v, C = $1/\dot{\varepsilon}_o$ and σ and $\dot{\varepsilon}$ have been equated to the yield stress σ_y and applied strain rate $\dot{\varepsilon}_y$, respectively, measured at the peak or plateau of the stress-strain curve. Hence plots of σ_y/T against log $\dot{\varepsilon}_y$ at different temperatures should be linear and parallel, having a slope characterised by A and intercepts determined by the values of C and Q.

Various studies[3,4] of the yield behaviour of amorphous glassy polymers have shown that the yield stress increases more rapidly with increasing strain rate and decreasing temperature at low temperatures and high strain rates than at high temperatures and low strain rates. An extension to equation (13) has therefore been proposed based on the assumption that the yield stress comprises additive contributions from the glass-rubber α relaxation process and the secondary β process. The extended equation is then

$$\frac{\sigma_y}{T} = A_\alpha[\ln 2C_\alpha\dot{\varepsilon}_y + (Q_\alpha/RT)] + A_\beta \sinh^{-1}[C_\beta\dot{\varepsilon}_y \exp(Q_\beta/RT)] \qquad (14)$$

As illustrated in Figure 2, the β contribution to σ_y/T is represented by an inverse sinh function. This follows from (12a) recognising that at certain rates and temperatures $\sigma v/RT$ for the β process will be small or zero. At a given temperature (fig 2), the plot of σ_y/T versus log $\dot{\varepsilon}_y$ exhibits limiting slopes at low and high strain rates determined by the values of A_α and $A_\alpha + A_\beta$ respectively.

5 EXPERIMENTAL

5.1 MATERIALS

The materials used in this investigation are listed in Table 1 and are identical to those for which data have previously been reported[1]. They comprise polycarbonate, a propylene-ethylene copolymer containing 8 wt% ethylene and an acrylonitrile-butadiene-styrene copolymer (ABS).

Table 1 - Materials Investigated

Plastic	Supplier/Code No
Polycarbonate	Bayer, Macrolon 293
Propylene-ethylene copolymer	BASF, Novolen 2300LL
ABS	BASF, Terluran 967K

The polycarbonate was obtained in the form of sheets of thickness 3 mm. The propylene-ethylene copolymer and ABS were supplied as pellets from which compression moulded sheets of thickness 3.2 mm were produced.

Both tensile and shear tests were carried out on specimens machined from the sheets. Standard dumbbell-shaped specimens (ISO 3167) and Arcan V-notched square plates were used in the tensile and shear tests, respectively, at low strain rates[1] (Section 5.2). The tensile tests at high strain rates (Section 5.3) employed dumbbell-shaped specimens of overall length 75 mm and width of 5 mm in the narrow gauge section.

5.2 MEASUREMENTS AT LOW STRAIN RATES (10^{-5} - 10^{-1} s^{-1})

Both tensile and shear tests at low strain rates were carried out using an Instron universal testing machine type 4505. The measurements were made at 50, 23 and 0 °C for each material.

5.2.1 Tensile Measurements

For the determination of Young's modulus E and Poisson's ratio ν_e, extensometers[1,5] were employed to measure longitudinal strains over a 50 mm gauge length and transverse strains (in the width direction) were measured using an Instron clip-on extensometer. Values of E and ν_e were usually derived from data over the strain range 0.0005→0.0025 and were reproducible to within about ±1% and ±3% respectively.

For determining stress-strain curves and Poisson's ratio over wide ranges of strain up to failure, both longitudinal and transverse strains were measured using a Messphysik ME64 videoextensometer. Details of these measurements are included in reference 1 together with a discussion of their use in studying the non-uniform deformation during tensile yielding in polycarbonate and the propylene-ethylene copolymer. Particular emphasis was given to calculating the required local stresses and strains in the neck region of polycarbonate specimens, and correcting for a marked increase in the local strain rate during neck propagation[1].

5.2.2 Shear Measurements

Shear stress-strain data were obtained from measurements on Arcan notched-plate specimens with the aid of extensometers developed at the NPL[1,6]. The results were corrected for non-uniformities in stress and strain within the specimens on the basis of finite-element calculations[1].

5.3 TENSILE MEASUREMENTS AT HIGH STRAIN RATES (10^{-2}-100 s^{-1})

5.3.1 Measurements with a Servohydraulic Machine

An Instron 1143 servohydraulic test machine was used to generate tensile data at crosshead speeds between about 0.1 mm s^{-1} and 2 ms^{-1}, corresponding to strain rates in the range 10^{-2}-40 s^{-1}. Loads were measured using a lightweight Kistler piezo-electric load cell with a 50 kN force capacity. Crosshead displacements were determined using a LVDT transducer built into the test machine. At strain rates up to about 1 s^{-1}, strains were measured using Instron clip-on extensometers having a 25 mm gauge length and 2.5 mm travel. The outputs from the load cell, displacement transducer and extensometers were recorded on a Gould Data Systems 840 digital storage oscilloscope with 16 bit resolution. The data were transferred to a PC for analysis using Gould Transfer Acquisition (v2.10.12) software.

At the lower strain rates, plots of strain versus crosshead displacement were modelled using a quadratic function[7]. For each material, the model parameters had little sensitivity to strain rate and were thus employed to calculate strains from the displacement measurements in high-rate tests. For some high-rate tests, these calculated strains were compared with strains determined using a high-rate extensometer based on a linescan camera[8]. Provided that the specimen does not form a neck during extension, these checks indicated that the strains estimated from the crosshead displacement are reliable.

5.3.2 Measurements with Impact Apparatus

A Rosand IFW5 falling weight impact machine with a tensile test frame[9] was used to generate data at impact velocities between 1 ms^{-1} and 4 ms^{-1} (strain rates 25-100 s^{-1}). With this apparatus, a falling weight strikes the free-hanging lower grip of the specimen clamped at its upper end to the frame. The force transmitted through the specimen was measured by a 50 kN Kistler piezo-electric force transducer attached to the top of the specimen frame and the fixed upper grip. The force signal was recorded on a computer that controls the impact apparatus, and was analysed using Rosand IFW5 (v1.08) software. The displacement of the grips was calculated from the test time and the initial impact velocity. Strains were determined from these displacements using the model functions derived from the tests on the servohydraulic machine.

5.3.3 Identification of Data Sets and Corrections to Strain Values

The peak or plateau yield stresses obtained from repeated high-rate tests at a given strain rate were typically scattered by $\pm$3% about the mean value. To aid in the subsequent analysis and presentation of data, those stress-strain data sets were thus identified for which the peak or plateau stress was close to the mean value within each scatter band.

Several of the high-rate data sets exhibited errors apparently associated with the inaccurate synchronisation of the force-time and displacement-time recordings at the start of the test. Figure 3 exemplifies typical results obtained with the servohydraulic machine, and illustrates the constant positive increment added to each strain value to ensure that the initial linear region of the stress-strain curve passed through the origin. Stress-strain curves obtained with the impact apparatus often showed an initial region of low slope and positive curvature, possibly resulting from the finite time for a stress wave pulse to travel along the specimen or from the take-up of slack within the loading train. Figure 4 illustrates this behaviour and the constant negative correction applied to each strain value.

5.3.4 Estimation of Transverse Strains and True Stresses

Values of the transverse engineering strain ε_t' were required for the calculation of true tensile stresses, $\sigma_T = \sigma'/(1+\varepsilon_t')^2$, from the measured engineering stresses σ'. Since transverse strains were not determined in the high-rate tests, values were estimated from the longitudinal engineering strains ε' using relationships established from the low-rate tests. As exemplified in Figure 5, plots of ε_t' versus ε' could be described approximately in terms of two linear functions that intersected at a value of ε' denoted by ε^*, ie

$$\varepsilon_t' = -\nu_1\varepsilon' \quad (\text{for } \varepsilon' \leq \varepsilon^*) \tag{15a}$$

$$\varepsilon_t' = -\nu_1\varepsilon^* - \nu_2(\varepsilon' - \varepsilon^*) \quad (\text{for } \varepsilon' > \varepsilon^*) \tag{15b}$$

where $-\nu_1$ and $-\nu_2$ are the respective slopes of the two regions. Table 2 lists the average values of ν_1, ν_2 and ε^* determined over the strain rate range 10^{-4}-10^{-1} s^{-1} and temperature range 0-50 °C, and we note that for each material ε^* is close to the strain at which a peak was observed in Poisson's ratio[1]. In the case of polycarbonate, this peak was very broad and marked the onset of strain hardening during yield, whereas for the propylene-ethylene copolymer and ABS the peak was sharp and resulted from cavitation. Note also that whilst ν_1 was essentially constant, the values of ν_2 and ε^* were material dependent and varied significantly with strain rate and temperature. Although the experimental scatter was too large to permit accurate extrapolations to high rates and low temperatures, the ε_t' (and hence σ_T) values obtained using low-rate values of ν_2 and ε^* are considerably more reliable at high strains than values estimated assuming a constant Poisson's ratio.

Table 2 - Values of Parameters Characterising the Variation of ε_t' with ε'

Material	ν_1	ν_2	ε^*
Polycarbonate	0.42	0.24	0.29
Propylene-ethylene copolymer	0.40	0.10	0.05
ABS	0.42	0.06	0.02

6 RESULTS AND DISCUSSION

6.1 ELASTIC MODULI AND POISSON'S RATIOS

Accurate values of E and ν_e were obtained only in the low strain rate region at temperatures of 0, 23 and 50 °C (see Section 5.2.1). From the results for polycarbonate shown in Figure 6 it is found that E increases by about 1% per decade increase in strain rate and by about 0.2% per °C decrease in temperature. At each temperature the plots show a negative curvature reflecting the approach to the glassy plateau with increasing strain rate following the rubber-glass relaxation region. Somewhat larger variations are observed in Figure 7 for ABS (1.75%/decade; -0.3%/°C), the results again being consistent with the approach to the glassy plateau region of an amorphous polymer.

Much larger modulus variations are observed for the propylene-ethylene copolymer (Fig 8), averaging about 13%/decade and -2%/°C over the temperature range studied. The rate

dependence is particularly marked at 50 °C, reflecting the α crystalline relaxation process, and at 0 °C due to the onset of the rubber-glass relaxation and associated stiffening of the amorphous phase with increasing rate. The modulus plateau separating the α and β relaxation regions is evident at the high-rate end of the plot at 23 °C.

The average ν_e values for polycarbonate and ABS were about 0.39 and 0.38 respectively, no systematic trends being observed with strain rate or temperature within the reproducibility of ±3%. For the propylene-ethylene copolymer, ν_e decreases substantially with increasing strain rate and decreasing temperature (Fig 9), consistent with the influence of α and β relaxation processes.

The dependence of E and ν_e on strain rate and temperature could in principle be modelled in terms of parameters obtained from stress relaxation data. Such analyses would be somewhat complicated by the overlap of different relaxation regions and have not been undertaken in this project.

6.2 TENSILE STRESS-STRAIN CURVES

For each polymer investigated, families of tensile stress-strain curves have been generated covering strain rates in the range 10^{-4}-100 s^{-1} at temperatures of 50, 23, 0 and -40 °C respectively. From the results for polycarbonate, presented in Figures 10a-d, a peak in stress is generally observed at a strain around 0.05-0.1. The peak increases in height and shifts to higher strains with increasing strain rate and decreasing temperature. The fall in stress (strain softening) at strains above that associated with the peak coincides with the appearance of a neck within the specimen during yielding under tension. For the three lowest strain rates at 50, 23 and 0 °C, the method of analysis described previously[1] was used to determine the local stress and strain within the neck region during its formation and propagation along the specimen. These analyses revealed that the stress falls quite sharply following the peak, remains essentially constant for strains up to about 0.3 and then shows a progressive increase (strain hardening). At the higher strain rates, no reliable data were obtained at strains much higher than that associated with the peak since the techniques did not allow local strain measurements within the neck region. Based on the behaviour at lower strain rates, however, it is assumed that the shape of the stress-strain curve does not vary much with strain rate or temperature.

Results for the propylene-ethylene copolymer are presented in Figures 11a-d. At the higher temperatures and lower strain rates, the stress increases smoothly with strain to a maximum level that remains essentially constant during yield. This stress level increases with increasing rate and decreasing temperature. Similar results are observed at lower temperatures and higher rates, except that a gradual decrease in stress with strain (strain softening) is observed after attaining the maximum at a strain value (0.02-0.08) that decreases with increasing rate and decreasing temperature.

Figures 12a-d show the stress-strain curves obtained for ABS. At the higher temperatures and lower strain rates, a peak is observed in the curves at a strain of about 0.02. With increasing strain above that associated with the peak, strain softening is observed by a sharp fall in the stress to a constant level or plateau that is maintained over a wide strain range up to failure. Both the peak height and the plateau stress level increase with increasing rate and decreasing temperature. The rate of this increase is greater for the plateau stress than for the peak stress so that the strain softening effect is reduced and finally eliminated.

6.3 EFFECTIVE STRESS-STRAIN CURVES FROM SHEAR DATA. COMPARISON WITH TENSILE CURVES

Plots of the effective stress $\bar{\sigma}$ versus effective strain, $\bar{\varepsilon}=\bar{\varepsilon}_p+(\bar{\sigma}/E)$, were calculated from shear σ_s and γ_p values using equations (8) and (9), assuming that the values previously derived[1] for λ are independent of strain rate and temperature. For polycarbonate, the calculated plots using λ=1.1 were, as expected, closely similar to the tensile stress-strain curves at corresponding effective strain rates and temperatures, since tensile yielding is dominated by shear deformation[1].

The calculations of $\bar{\sigma}$ and $\bar{\varepsilon}$ for the propylene-ethylene copolymer and for ABS were based on a λ value of 1.2, obtained from compression and shear data using equation (11). At each temperature and strain rate (Figs 13a-c, 14a-c), $\bar{\sigma}$ increases smoothly with $\bar{\varepsilon}$ to a maximum value and then remains constant or decreases slightly over a wide strain range. The maximum value of $\bar{\sigma}$ is seen to increase progressively with increasing rate and decreasing temperature.

Figure 15 compares $\bar{\sigma}$ versus $\bar{\varepsilon}$ curves derived from shear data with the tensile stress-strain curves for the propylene-ethylene copolymer at corresponding temperatures and effective strain rates $\dot{\bar{\varepsilon}}$. At 50 °C and low effective strain rate (0.0003 s^{-1}) the tensile curve lies only slightly below the shear curve, suggesting that tensile yielding is dominated by shear deformation which could be accompanied by some crazing or rubber particle cavitation. At 0 °C and a higher effective strain rate (0.03 s^{-1}) much larger deviations are observed, indicating a substantial contribution to the tensile yielding from crazing or rubber particle cavitation which initiates at a strain level around 0.02.

A similar data comparison for ABS (Fig 16) reveals rather larger deviations between the effective stress-strain curves from tension and shear, these deviations again increasing with decreasing temperature and increasing rate. For this material, the effects of cavitation seem to have a prominent influence on the tensile yield behaviour for all rates and temperatures so far investigated. Assuming that matrix crazing is the dominant cavitation mechanism then, under conditions for which shear yielding may be neglected, the tensile stress-strain curves may be identified with plots of $\bar{\sigma}^c$ versus $\bar{\varepsilon}^c\ (=\bar{\varepsilon}_p^c+\varepsilon_e)$.

6.4 DEPENDENCE OF PEAK OR PLATEAU STRESSES ON STRAIN RATE AND TEMPERATURE

Figure 17 shows plots of σ_y/T versus log $\dot{\varepsilon}_y$ for polycarbonate obtained from the peak tensile stresses and strain rates at -40, 0, 23 and 50 °C respectively. It will be observed that the plots are well-fitted by equation (14) with the values of parameters given in Table 3. The values of A_α, Q_α and C_α are close to those reported by Bauwens-Crowet and coworkers[4] and the value of A_β is larger than that for A_α, a result consistent with the relatively small volume of the motional unit for the secondary β-process. Also note that the values of Q_β and C_β are typical of those obtained for secondary processes in glassy polymers using low-strain mechanical techniques[10]. In particular, the value of C_β is close to the reciprocal of a molecular vibration frequency. The shift direction required to superpose the plots in Fig 17 at different temperatures may be resolved into horizontal and vertical components determined by the values of Q_β and Q_α-Q_β respectively. The magnitude of the vertical component represents an effective scaling of stress values required to obtain superposition of stress-strain curves by a corresponding strain rate-temperature equivalence.

Table 3 - Values of Parameters Characterising the Dependence of Peak or Plateau Stresses on Strain Rate and Temperature

Material	Polycarbonate	Propylene-ethylene copolymer		ABS		
Test method	Tension	Tension	Shear (effective stress)	Tension (peak stress)	Tension (plateau stress)	Shear (effective stress)
$A_\alpha \times 10^3$ (MPa/°K)	4.24	3.50	5.43	5.58	7.47	7.47
$Q_\alpha \times 10^{-5}$ (J/mole)	3.23	2.51	2.49	1.75	1.53	1.92
C_α (s)	2.00×10^{-31}	4.06×10^{-31}	1.97×10^{-33}	3.92×10^{-20}	2.35×10^{-19}	9.22×10^{-24}
$A_\beta \times 10^3$ (MPa/°K)	16.0	6.49				
$Q_\beta \times 10^{-5}$ (J/mole)	0.65	1.45				
C_β (s)	1.07×10^{-13}	3.01×10^{-27}				

The σ_y/T versus log $\dot{\varepsilon}_y$ plots derived from the maximum tensile stresses and corresponding strain rates for the propylene-ethylene copolymer are presented in Figure 18. Good fits are again obtained to the data using equation (14) with the values of parameters in Table 3. Differences between the values of corresponding parameters for the α and β processes are less marked than for polycarbonate, a result consistent with the fact that each process involves quite long-range molecular rearrangements. The shift direction required to superpose the σ_y/T versus log $\dot{\varepsilon}_y$ plots at different temperatures is indicated in Figure 18 and it appears from Figures 11a-d that this equivalence of strain rate and temperature enables stress-strain curves at different rates and temperatures to be superposed through a scaling of axes, avoiding changes in shape of the curves.

Figure 19 shows plots of $\bar{\sigma}_y / T$ versus log $\dot{\bar{\varepsilon}}_y$ obtained from the shear data for the propylene-ethylene copolymer. A reasonable fit to the data is obtained using a single Eyring function (equation (13)) for the α-process, although a slight underestimate of $\bar{\sigma}_y / T$ values at 0 °C could partly reflect a small contribution from the β-process. Although the values of A_α (Table 3) are larger than those obtained from the tensile data, the values of Q_α obtained from tension and shear agree within 1%, indicating a close connection between the mechanism of shear yielding and the initiation of cavitation.

Figures 20 and 21 show the σ_y/T versus log $\dot{\varepsilon}_y$ plots for ABS obtained from the respective peak and plateau stress levels, and associated strain rates, of the tensile stress-strain curves (Figs 12a-d). At the higher strain rates and lower temperatures, for which the strain softening effect, and thus distinct peaks, were no longer observed, peak stresses were taken as the measured stresses at strain levels estimated by linear extrapolation of peak strains as a function of rate and temperature. The plateau stresses were then taken as the measured stresses at high strains where the gradual strain hardening effect became negligible. Although the plots in Figures 20 and 21 have a slight tendency to upward curvature, the data for peak and plateau stresses are each quite well fitted by a single Eyring function

using the respective values of A_α, Q_α and C_α given in Table 3. Yield stress contributions from any secondary process in the styrene-acrylonitrile polymer matrix thus seem negligible. Since the plots at different temperatures in Figures 20 and 21 are parallel they could be superposed by shifting along any direction. However, for directions indicated by the broken lines, the shapes of stress strain curves having a corresponding strain rate-temperature equivalence seem to be approximately preserved.

Plots of $\overline{\sigma}_y / T$ versus log $\dot{\overline{\varepsilon}}_y$ obtained from the shear data for ABS are presented in Figure 22. These data can again be fitted by a single Eyring function and the derived value for A_α (Table 3) is identical to that obtained from the tensile plateau stress data. This indicates a close connection between the mechanism of shear yielding and dilatational yielding under tension.

From the successful application of the generalised Eyring model to the tensile and shear results, it follows that accurate predictions could be made of the peak or plateau yield stresses at impact rates (100 s^{-1}). This could involve either an extrapolation of results obtained at a given temperature, or a rate-temperature shift procedure using data obtained at different rates and temperatures. With the rate-temperature equivalence scheme, predictions of the shape of stress-strain curves at impact rates may be made, if guided by the shift directions indicated in Figures 17, 18 and 20.

6.5 STRAIN RATE AND TEMPERATURE DEPENDENCE OF λ and $\tan \psi$

Values of λ and $\tan \psi$ were estimated for each material over the range of effective strain rate (0.0003→0.05 s^{-1}) and temperature (0→50 °C) for which both tensile and shear data were obtained and for which transverse as well as longitudinal strains were determined in the tensile tests.

For polycarbonate, values of λ calculated from the peak tensile and shear stresses using equation (10) showed no systematic variations with strain rate or temperature. An average value of $\lambda = 1.14 \pm 0.03$ was obtained which compares with the value $\lambda = 1.07$ previously obtained[1] from compressive and tensile data at 23 °C. Values of $\tan \psi$ obtained from the tensile data for polycarbonate using equation (5) were close to zero ($0 \leq \tan \psi < 0.2$) over the range of strain, strain rate and temperature investigated. The tensile yielding thus occurs at constant volume or produces only a small volume increase. We conclude that the tensile, shear and compressive behaviour of polycarbonate involves a predominantly shear mechanism having a small sensitivity to the hydrostatic stress component ($\lambda \approx 1.1$) that is essentially independent of strain rate and temperature.

For the propylene-ethylene copolymer and ABS, the λ values calculated from the peak or plateau tensile and shear stresses increased markedly with increasing strain rate and decreasing temperature. The values ranged from 1.3 to 2.9 for the propylene-ethylene copolymer and from 1.7 to 3.5 for ABS. Such variations undoubtedly arise from the increased contributions from cavitation to the tensile yielding. Hence the apparent λ values derived from tensile and shear data cannot be used to characterise the sensitivity of shear yielding to the hydrostatic stress component for these materials. It has therefore been assumed (see Section 6.3) that the value of $\lambda = 1.2$, obtained from compressive and shear data both for the propylene-ethylene copolymer and for ABS, is independent of strain rate and temperature. The volume increases associated with the cavitation during tensile yielding were directly reflected in the values of $\tan \psi$ calculated using equation (5). At a

given strain, tan ψ increased with increasing strain rate and decreasing temperature, attaining maximum values of 1.08 and 1.22 for the propylene-ethylene copolymer and ABS, respectively, at the highest rates and lowest temperatures investigated. These results could have an important bearing on our understanding of yielding mechanisms in cavitated polymers, and will be considered in future work aimed at improving existing models for the non-linear behaviour of plastics materials.

7 CONCLUSIONS

For each material investigated, the modulus E exhibits a significant dependence on strain rate and temperature. The modulus variations are most marked for the propylene-ethylene copolymer and for this material Poisson's ratio ν_e also varies significantly. The rate and temperature dependence of E could be modelled in terms of parameters obtained from stress relaxation data, but this may be complicated by the overlap of α and β relaxation regions.

The shapes of the tensile stress-strain curves for the propylene-ethylene copolymer and for ABS vary somewhat with strain rate and temperature. For these materials, differences are also observed between the tensile curves and the effective stress ($\bar{\sigma}$) versus effective strain ($\bar{\varepsilon}$) curves calculated from shear data (using λ = 1.2) at corresponding effective strain rates and temperatures. These differences increase with increasing rate and decreasing temperature, a result attributed to increased contributions from cavitation to the tensile yield process.

The dependence of peak or plateau yield stresses on strain rate and temperature can be described successfully in terms of Eyring's model. For polycarbonate and the propylene-ethylene copolymer, a generalised form of the model is required that accounts for contributions to the yield stress from α and β relaxation processes. Accurate predictions of the yield behaviour at impact rates can then be made by extrapolation or by the use of strain rate-temperature superposition.

- For polycarbonate, values of the shear yield parameters λ ($\approx$1.1) and tan ψ ($\approx$0) are essentially independent of strain rate and temperature. However, for the propylene-ethylene copolymer and ABS, apparent values of λ (calculated from tensile and shear data) and of tan ψ increase with increasing strain rate and decreasing temperature. These results reflect the increasing cavitation during tensile yielding which should be allowed for through an extension to existing models.

8 ACKNOWLEDGEMENTS

The work reported here forms part of a research programme on materials measurement and technology funded by the Department of Trade and Industry.

9 REFERENCES

B.E. Read, G.D. Dean and B.C. Duncan, Characterisation of the non-linear behaviour of plastics for finite element analysis. NPL report CMMT(A)114 (1998).

2. H. Eyring, J. Chem. Phys. 4 (1936), p 283.

3. J.A. Roetling, Polymer 6 (1965), p 311.

4. C. Bauwens-Crowet, J-C. Bauwens and G. Homès, J. Polym. Sci. A2, 7, (1969), p 735.

5. B.E. Read and G.D. Dean, Polymer 25 (1984) p 1679.

6. B.C. Duncan and G.D. Dean, Test Methods for determining shear property data for adhesives suitable for design. NPL report CMMT(B)56 (1996).

7. B.C. Duncan, Development of a high rate extensometer. NPL report CMMT(A)109 (1998).

8. B.C. Duncan, Methods for measuring strains at high rates. NPL report CMMT(A)133 (1998).

9. B.C. Duncan and A. Pearce, Comparison of impact and high rate tests for determining properties of adhesives and polymers needed for design under impact. NPL report CMMT(A)134 (1999).

10. N.G. McCrum, B.E. Read and G. Williams, Anelastic and dielectric effects in polymeric solids, Wiley, London (1967). Republished by Dover Publications Inc, New York (1991).

FIGURE CAPTIONS

Fig 1 The Eyring model.

Fig 2 Contributions to σ_y/T from the respective α and β relaxation processes according to the generalised Eyring model.

Fig 3 Illustration of the strain increment added as a correction to data from the servohydraulic machine.

Fig 4 Illustration of the negative strain increment applied as a correction to data from the impact apparatus.

Fig 5 Illustration of the parameters derived from modelling the variation of transverse engineering strain (ε_t') with engineering strain (ε') in terms of two linear regions.

Fig 6 Dependence of Young's modulus E on strain rate $\dot{\varepsilon}$ for polycarbonate at the temperatures indicated.

Fig 7 Dependence of Young's modulus on strain rate for ABS at the temperatures indicated.

Fig 8 Dependence of Young's modulus on strain rate for the propylene-ethylene copolymer at the temperatures indicated.

Fig 9 Dependence of Poisson's ratio ν_e on strain rate for the propylene-ethylene copolymer at the temperatures indicated.

Figs 10a-d Tensile stress-strain data for polycarbonate at the specified strain rates (s^{-1}) corresponding to the peaks in stress. Fig 10a, 50 °C; Fig 10b, 23 °C; Fig 10c, 0 °C; Fig 10d, -40 °C.

Figs 11a-d Tensile stress-strain data for the propylene-ethylene copolymer at the specified strain rates (s^{-1}) corresponding to the stress maxima. Fig 11a, 50 °C; Fig 11b, 23 °C; Fig 11c, 0 °C; Fig 11d, -40 °C.

Figs 12a-d Tensile stress-strain data for ABS at the specified strain rates (s^{-1}) corresponding to the peaks in stress. Fig 12a, 50 °C; Fig 12b, 23 °C; Fig 12c, 0 °C; Fig 12d, -40 °C.

Figs 13a-c Effective stress versus effective strain plots derived from shear data for the propylene-ethylene copolymer at the specified strain rates (s^{-1}) corresponding to the stress maxima. Fig 13a, 50 °C; Fig 13b, 23 °C; Fig 13c, 0 °C.

Figs 14a-c Effective stress versus effective strain plots derived from shear data for ABS at the specified strain rates (s^{-1}) corresponding to the stress maxima. Fig 14a, 50 °C; Fig 14b, 23 °C; Fig 14c, 0 °C.

Comparison of effective stress-effective strain curves determined from tensile data (filled points) and shear data (open points), respectively, for the propylene-ethylene copolymer. The temperatures and effective strain rates $\left[\dot{\bar{\varepsilon}}(s^{-1})\right]$ for the corresponding pairs of curves are as indicated.

Fig 16 Comparison of effective stress-effective strain curves determined for ABS from tensile data (filled points) and shear data (open points) respectively. The temperatures and effective strain rates $\left[\dot{\bar{\varepsilon}}(s^{-1})\right]$ for the corresponding pairs of curves are indicated.

Fig 17 Dependence of σ_y/T on log $\dot{\varepsilon}_y$ for polycarbonate at the temperatures indicated, where σ_y and $\dot{\varepsilon}_y$ are the peak tensile stress and corresponding strain rate respectively. The continuous lines were obtained by fitting equation (14) to the data, with the values of parameters in Table 3. The dashed line indicates the shift direction required to superpose the curves obtained at different temperatures.

Fig 18 Variation of σ_y/T with log $\dot{\varepsilon}_y$ for the propylene-ethylene copolymer at the temperatures indicated, where σ_y and $\dot{\varepsilon}_y$ are the maximum (peak or plateau) tensile stress and corresponding strain rate respectively. The continuous lines were obtained by fitting equation (14) to the data, giving the values of parameters in Table 3. The dashed line indicates the shift direction required to superpose the curves at different temperatures.

Dependence of $\bar{\sigma}_y / T$ on log $\dot{\bar{\varepsilon}}_y$ for the propylene-ethylene copolymer at the temperatures indicated, where $\bar{\sigma}_y$ and $\dot{\bar{\varepsilon}}_y$ are the maximum effective stress and corresponding effective strain rate obtained from the shear data (Figs 13a-c). The continuous lines were obtained by fitting equation (13) to the data giving the values of parameters in Table 3.

Fig 20 Dependence of σ_y/T on log $\dot{\varepsilon}_y$ for ABS at the temperatures indicated, where σ_y and $\dot{\varepsilon}_y$ are the peak tensile stress and corresponding strain rate respectively. The continuous lines were obtained by fitting equation (13) to the data giving the values of parameters in Table 3. The dashed line indicates the approximate rate-temperature equivalence required in superposing stress-strain curves obtained at different rates and temperatures, avoiding changes in their shape.

Fig 21 Dependence of σ_y/T on log $\dot{\varepsilon}_y$ for ABS at the temperatures indicated, where σ_y and $\dot{\varepsilon}_y$ are the plateau tensile stress and corresponding strain rate respectively. The continuous lines were obtained by fitting equation (13) to the data, giving the values of parameters in Table 3.

Fig 22 Variation of $\bar{\sigma}_y / T$ with log $\dot{\bar{\varepsilon}}_y$ for ABS at the temperatures indicated, where $\bar{\sigma}_y$ and $\dot{\bar{\varepsilon}}_y$ are the maximum effective stress and corresponding effective strain rate obtained from the shear data (Figs 14a-c). The continuous lines were obtained by fitting equation (13) to the data, giving the values of parameters in Table 3.

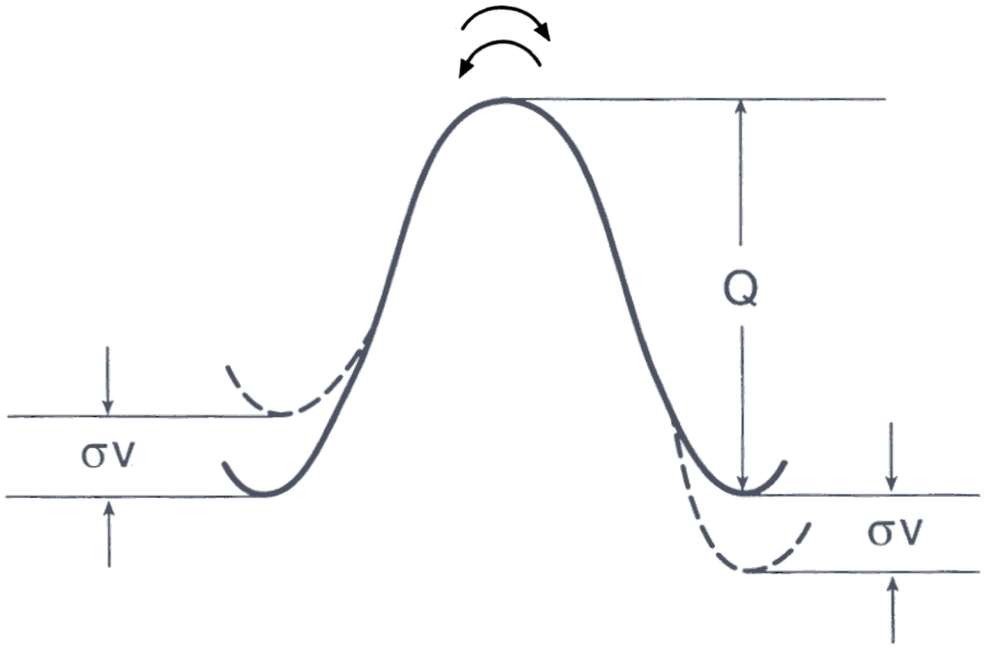

Fig.

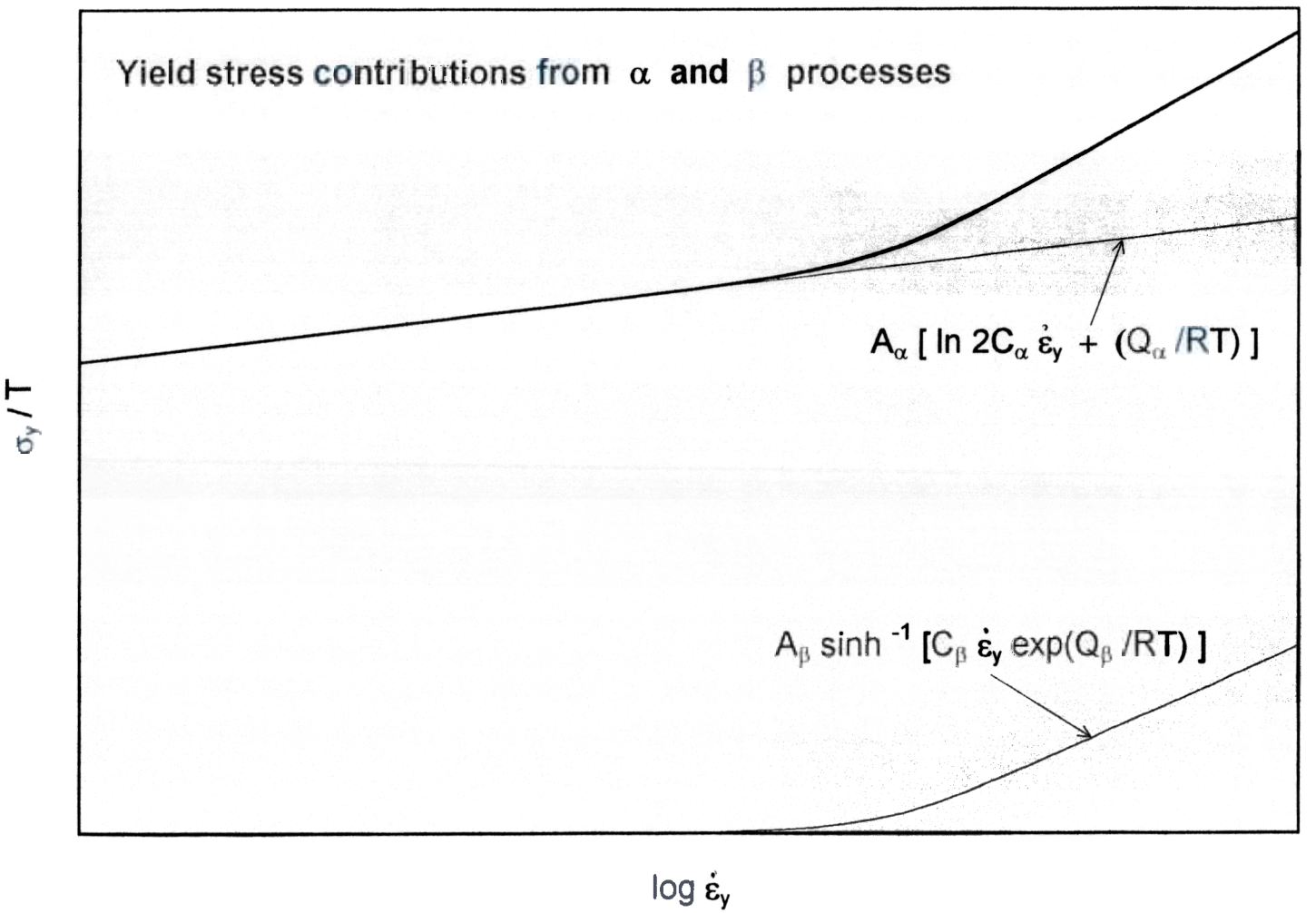
Yield stress contributions from α and β processes
A_α [ln $2C_\alpha \dot{\varepsilon}_y$ + (Q_α /RT)]
A_β sinh $^{-1}$ [$C_\beta \dot{\varepsilon}_y$ exp(Q_β /RT)]
σ_y / T
log $\dot{\varepsilon}_y$

Fig.

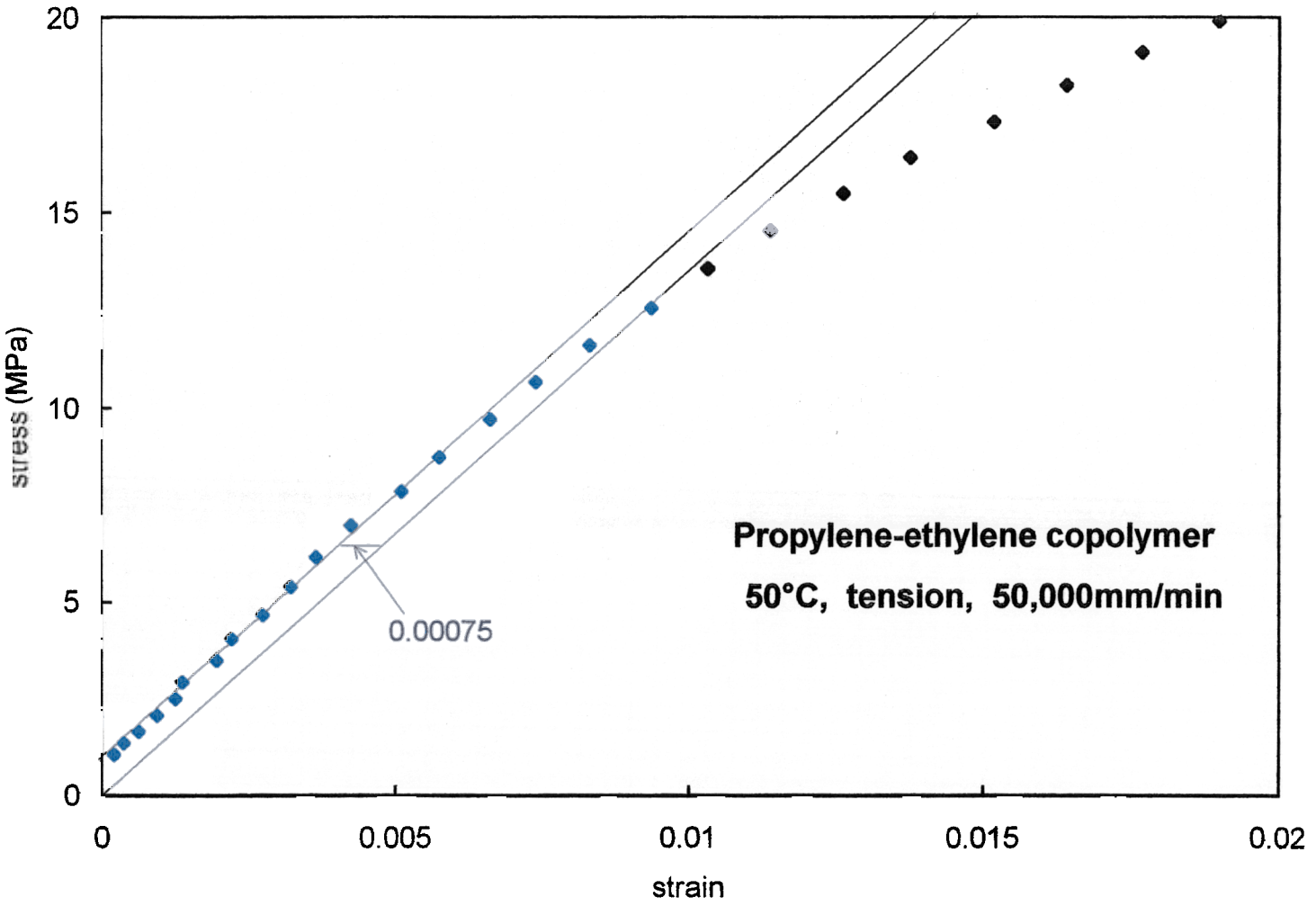
20
15
10
5
0
stress (MPa)
0
0.005
0.01
0.015
0.02
strain
0.00075
Propylene-ethylene copolymer
50°C, tension, 50,000mm/min

Fig. 3

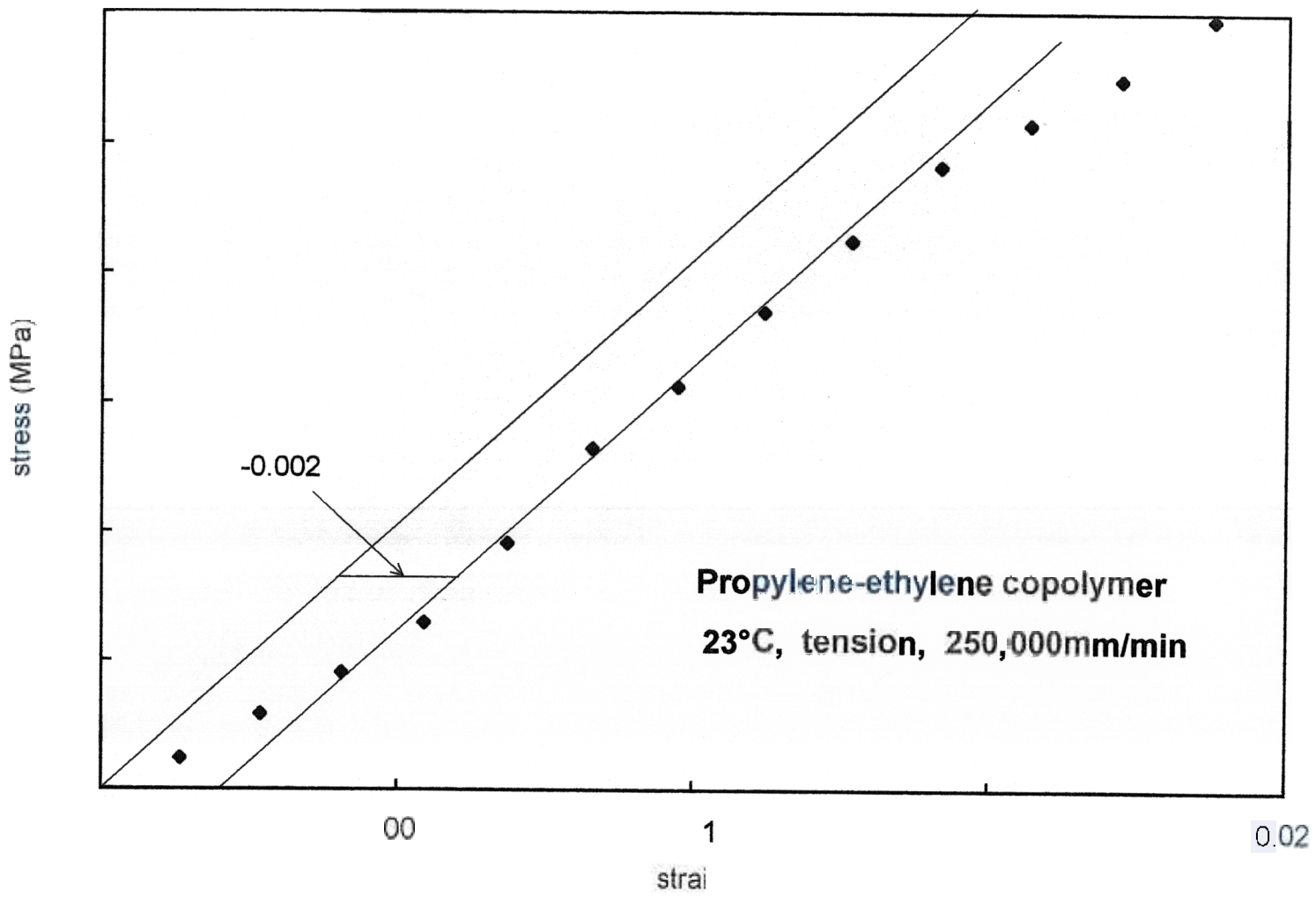
stress (MPa)
-0.002
Propylene-ethylene copolymer
23°C, tension, 250,000mm/min
00
1
0.02
strai

ig 4

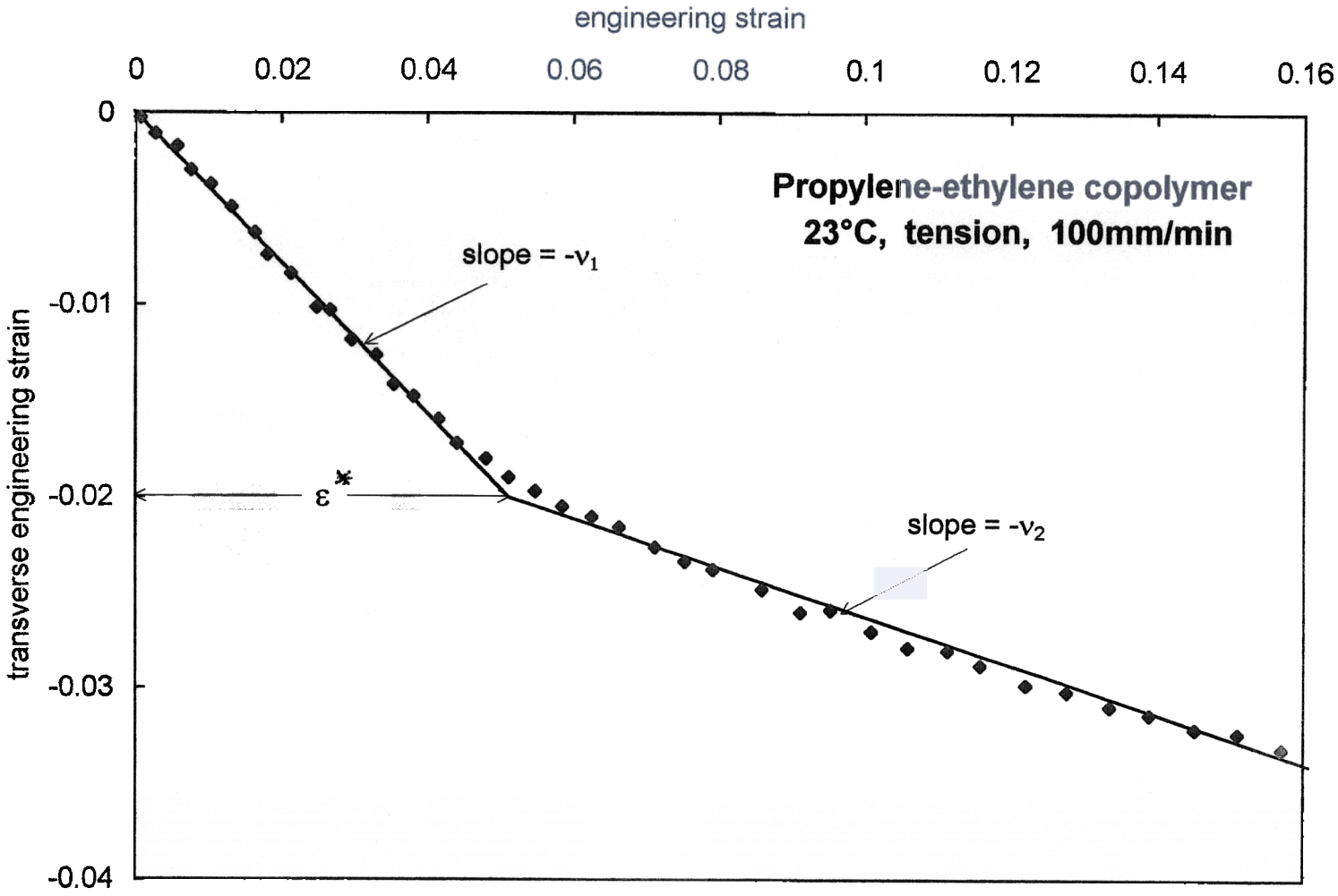
engineering strain
0
0.02
0.04
0.06
0.08
0.1
0.12
0.14
0.16
transverse engineering strain
0
-0.01
-0.02
-0.03
-0.04
Propylene-ethylene copolymer
23°C, tension, 100mm/min
slope = -ν1
ε*
slope = -ν2

Fig. 5

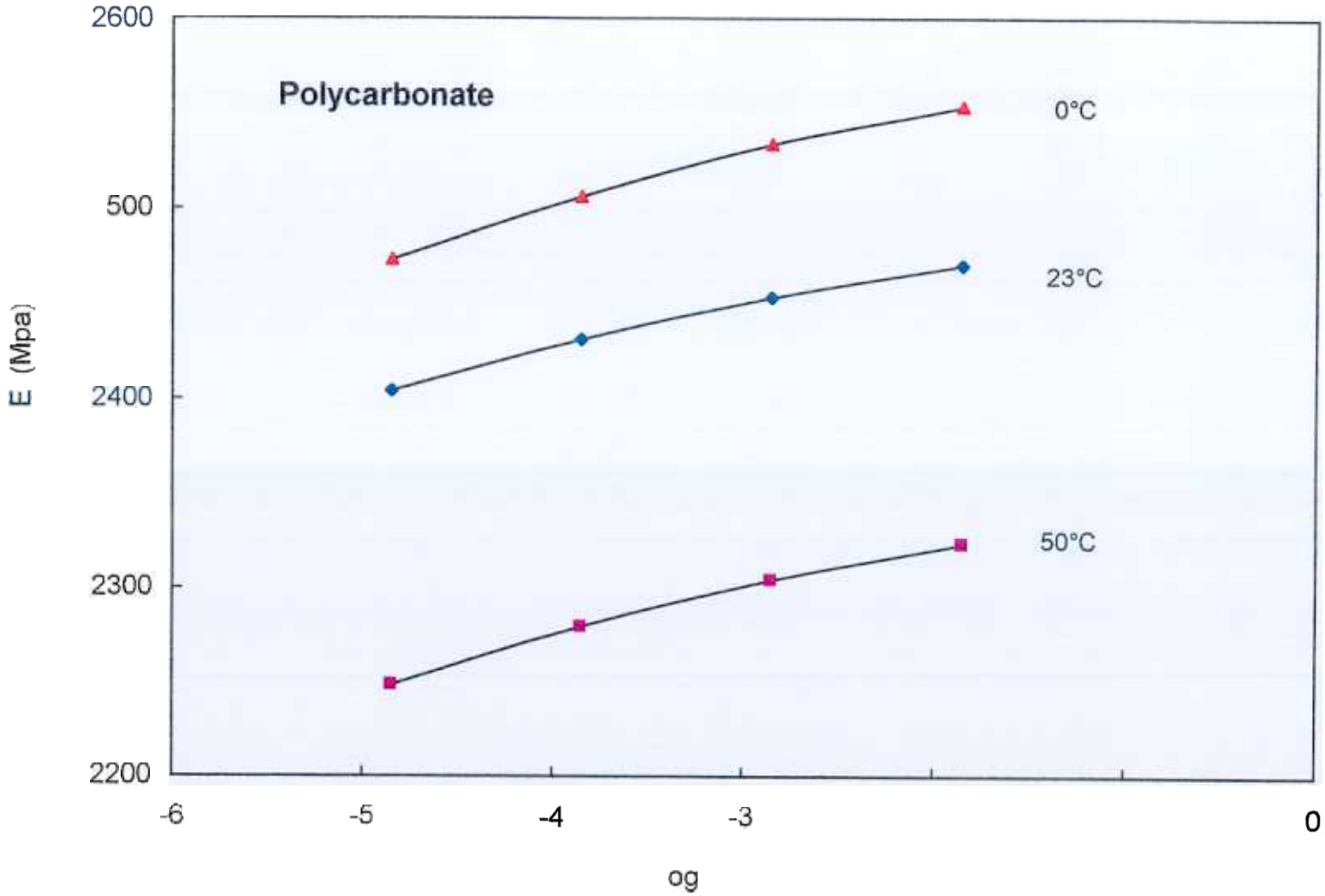
Polycarbonate
0°C
23°C
50°C
2600
500
2400
2300
2200
E (Mpa)
-6
-5
-4
-3
0
og

Fig. 6

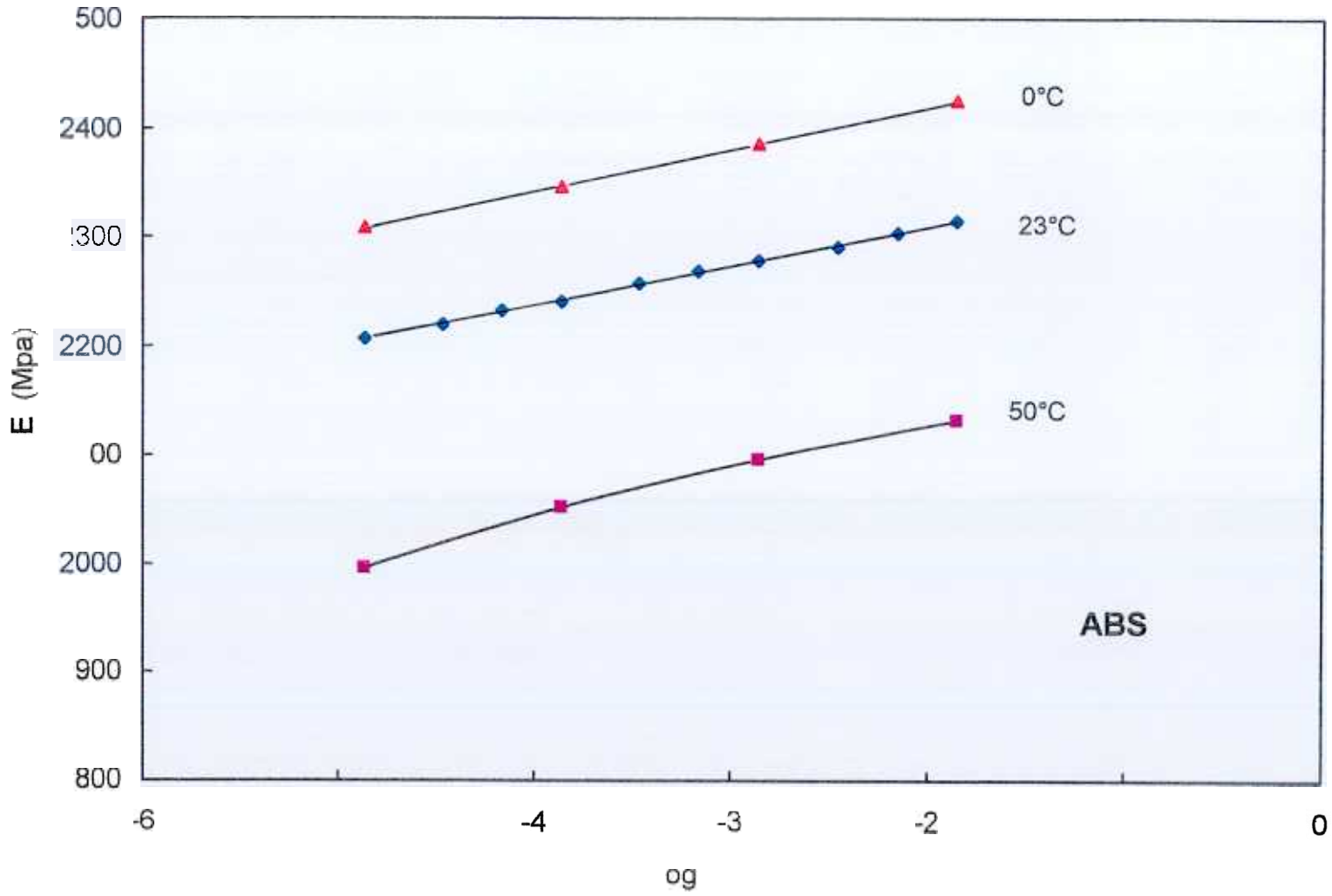

Fig. 7

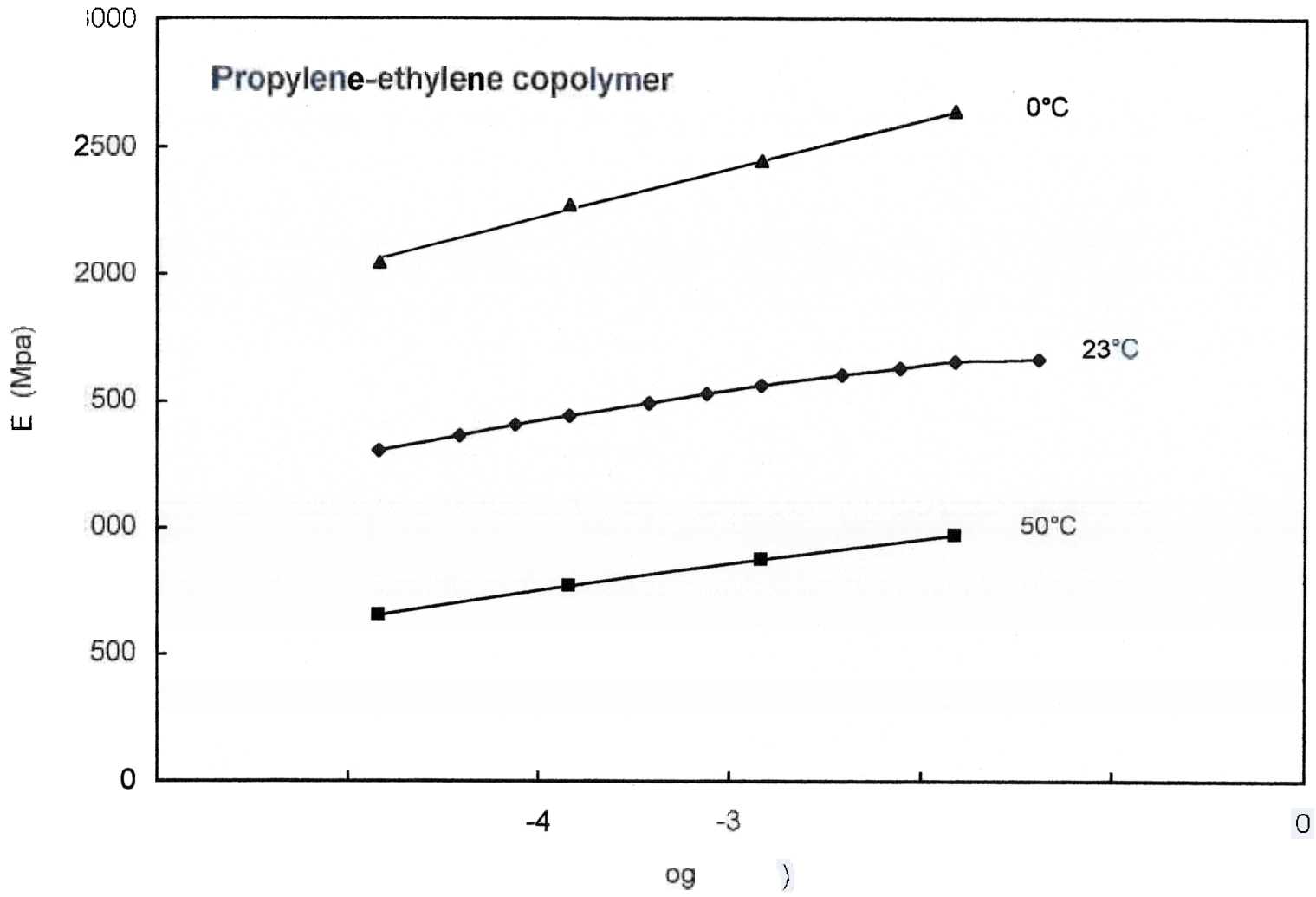
Propylene-ethylene copolymer
0°C
23°C
50°C
E (Mpa)
2500
2000
500
000
500
0
-4
-3
0
og
)

Fig 8

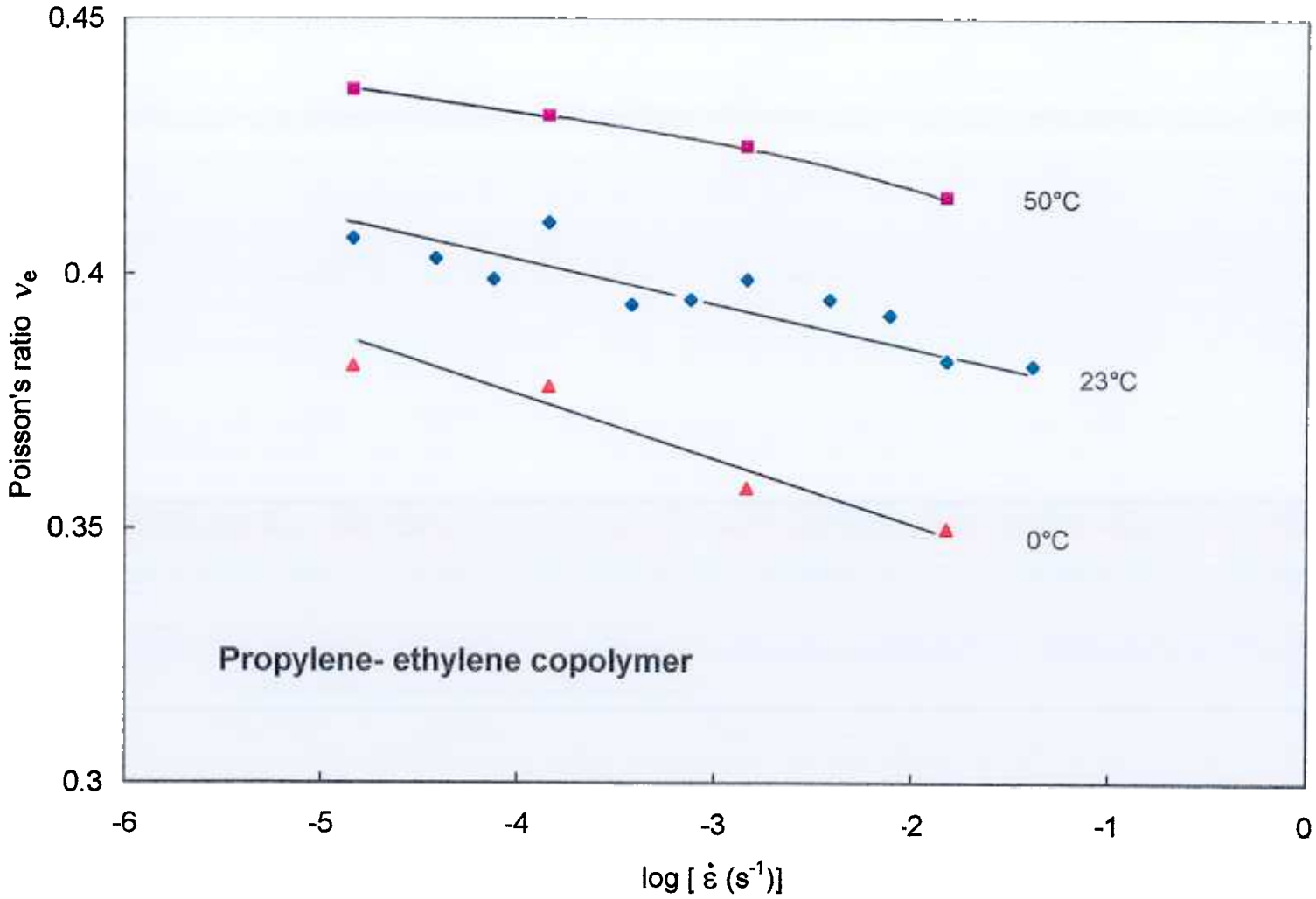
0.45
0.4
0.35
0.3
Poisson's ratio ν_e
-6
-5
-4
-3
-2
-1
0
log [$\dot{\varepsilon}$ (s^{-1})]
50°C
23°C
0°C
Propylene- ethylene copolymer

Fig. 9

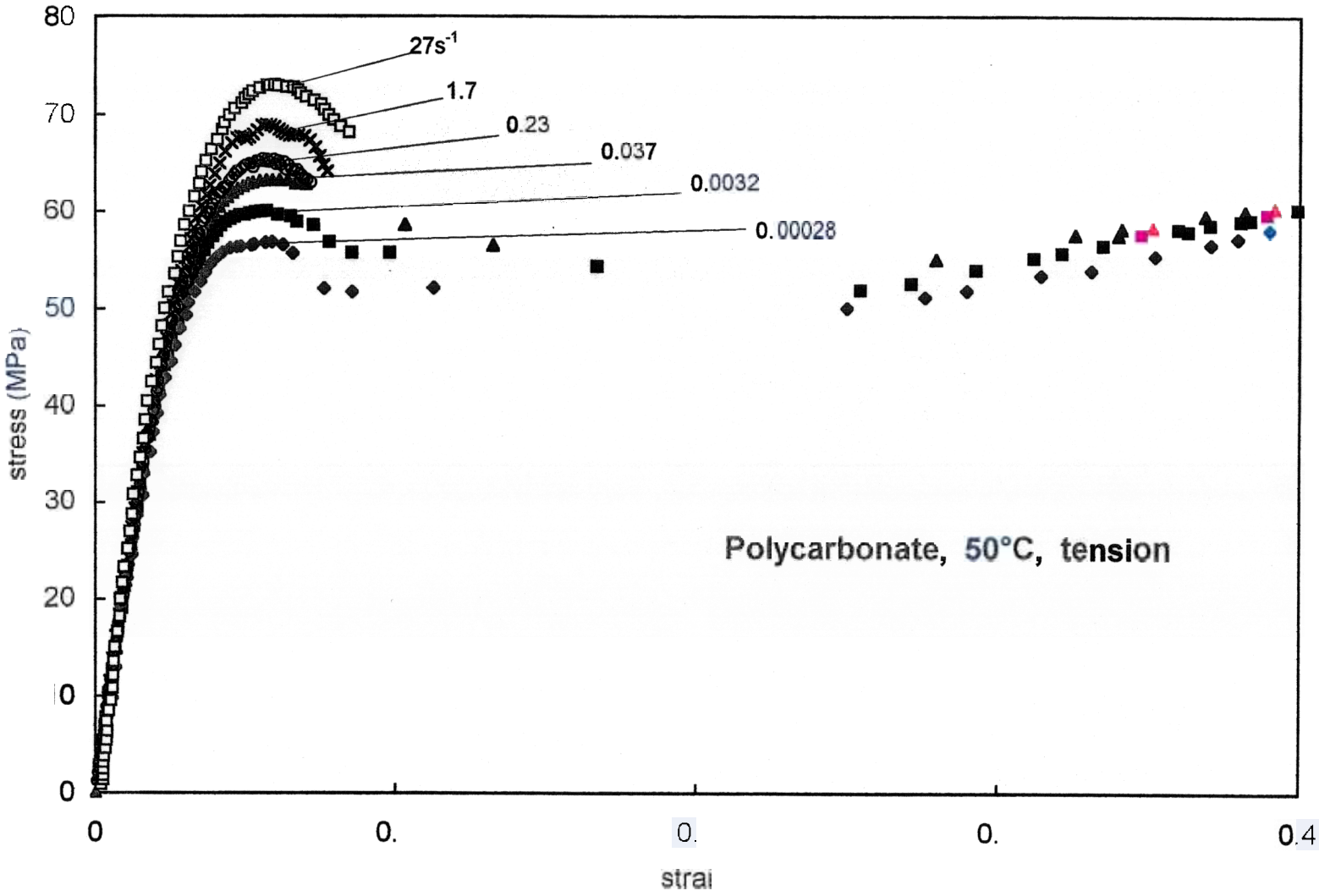
80
70
60
50
40
30
20
0
0
0
0.
0.
0.4
stress (MPa)
strai
27s-1
1.7
0.23
0.037
0.0032
0.00028
Polycarbonate, 50°C, tension

Fig. 0a

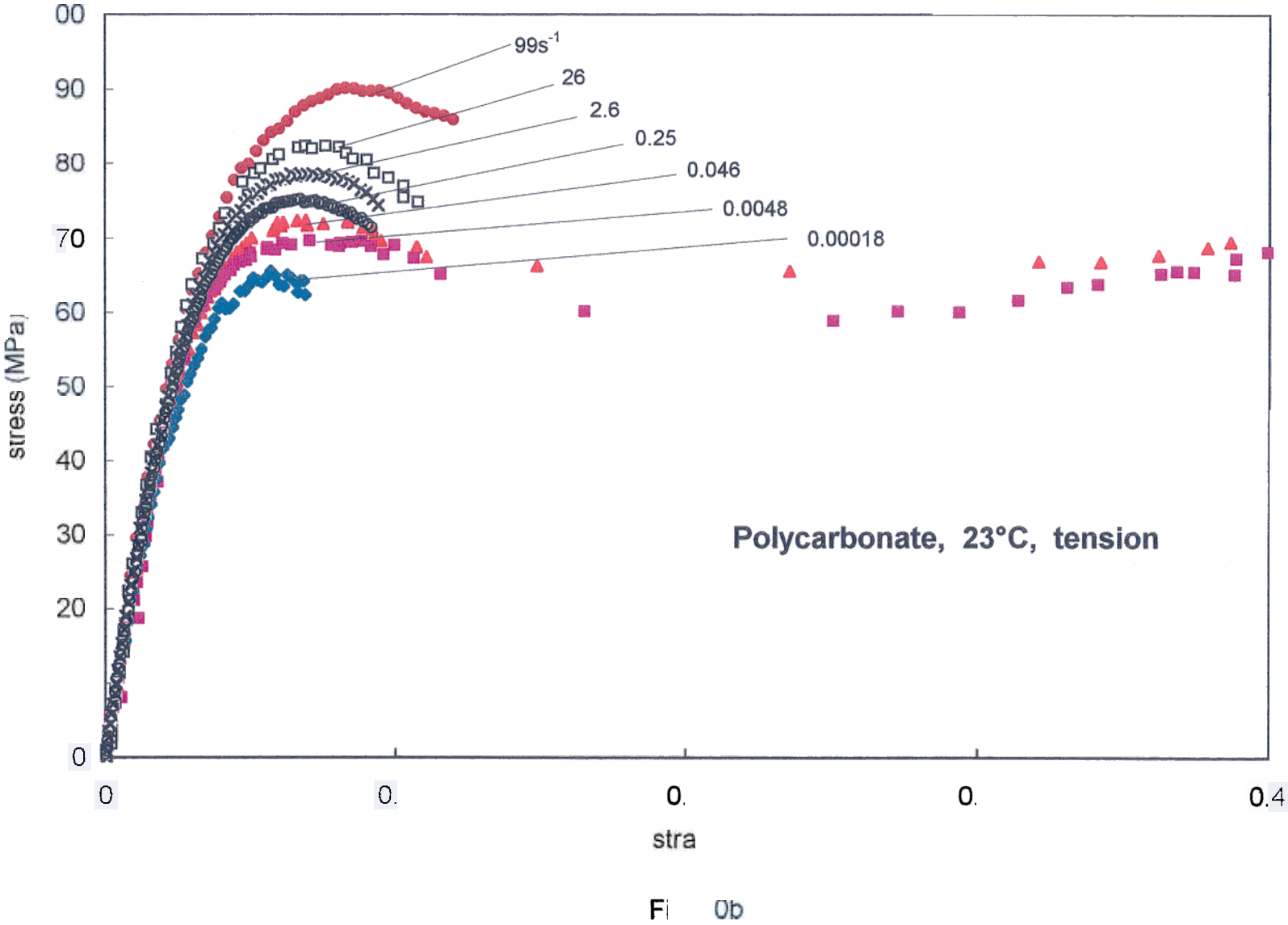
00
90
80
70
60
50
40
30
20
0
stress (MPa)
99s-1
26
2.6
0.25
0.046
0.0048
0.00018
Polycarbonate, 23°C, tension
0
0.
0.
0.
0.4
stra

Fi 0b

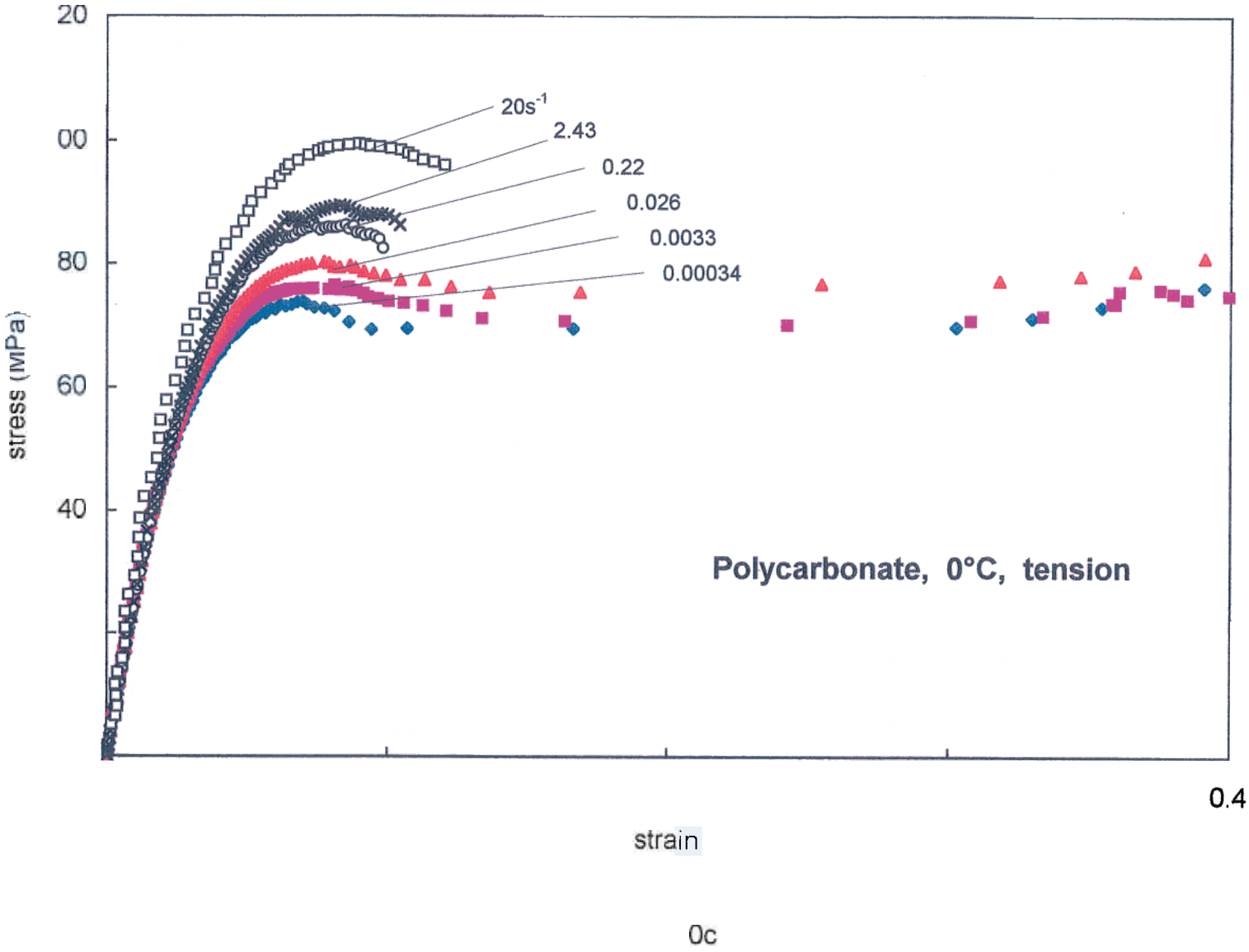
20
00
80
60
40
stress (MPa)
20s-1
2.43
0.22
0.026
0.0033
0.00034
Polycarbonate, 0°C, tension
0.4
strain
0c

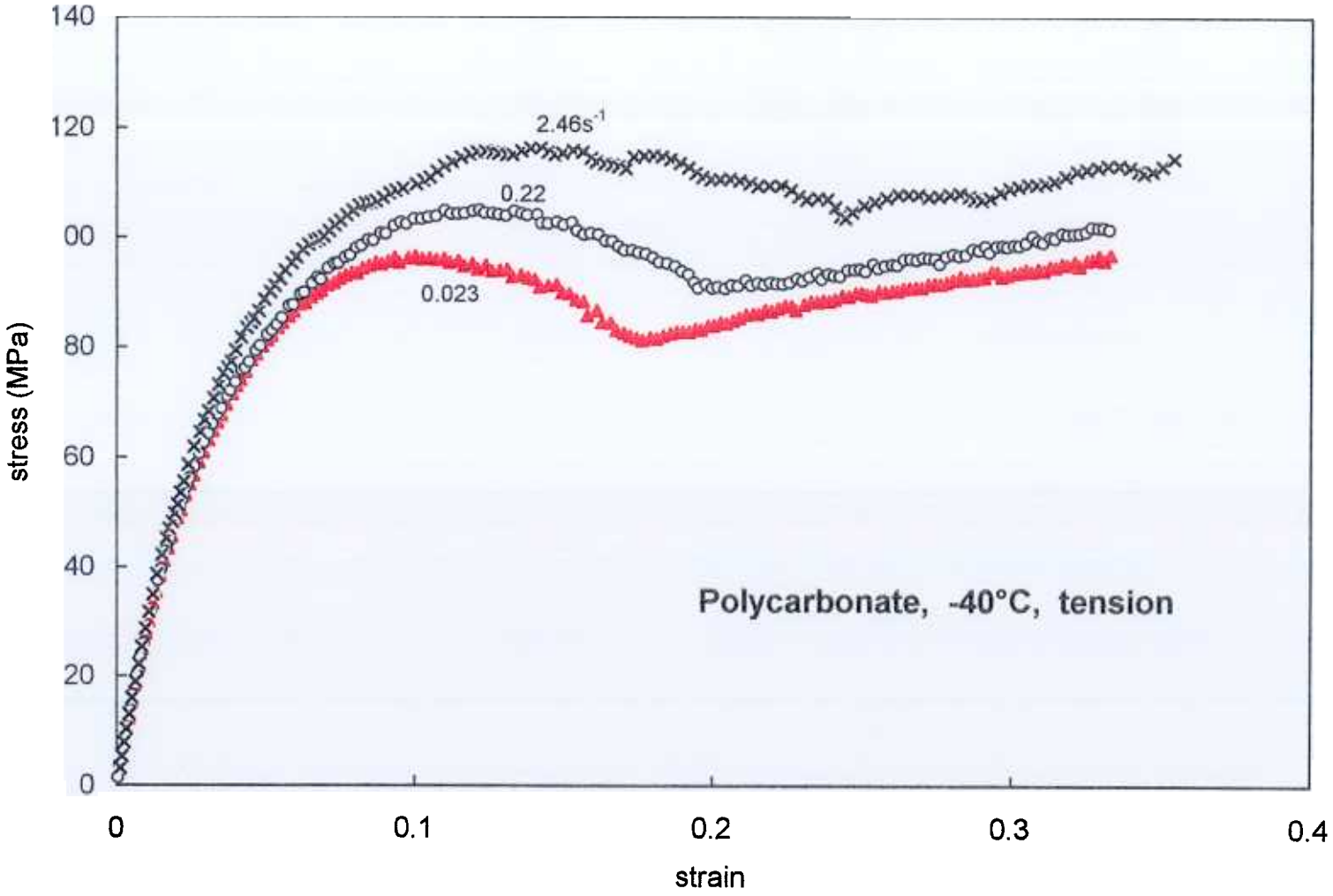
140
120
00
80
60
40
20
0
stress (MPa)
2.46s-1
0.22
0.023
Polycarbonate, -40°C, tension
0
0.1
0.2
0.3
0.4
strain

Fig. 10d

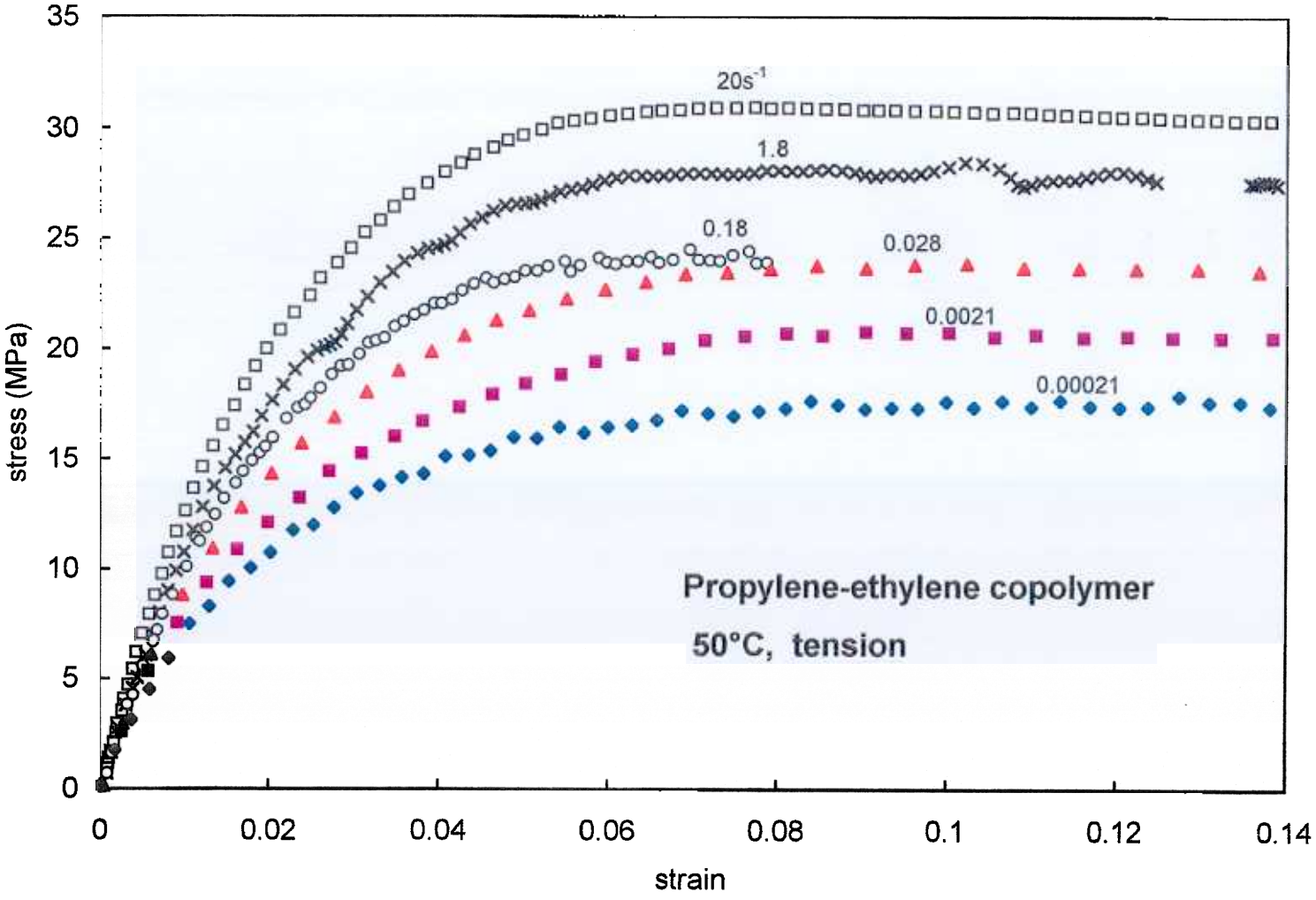
35
30
25
20
15
10
5
0
stress (MPa)
0
0.02
0.04
0.06
0.08
0.1
0.12
0.14
strain
20s-1
1.8
0.18
0.028
0.0021
0.00021
Propylene-ethylene copolymer
50°C, tension

Fig. 1a

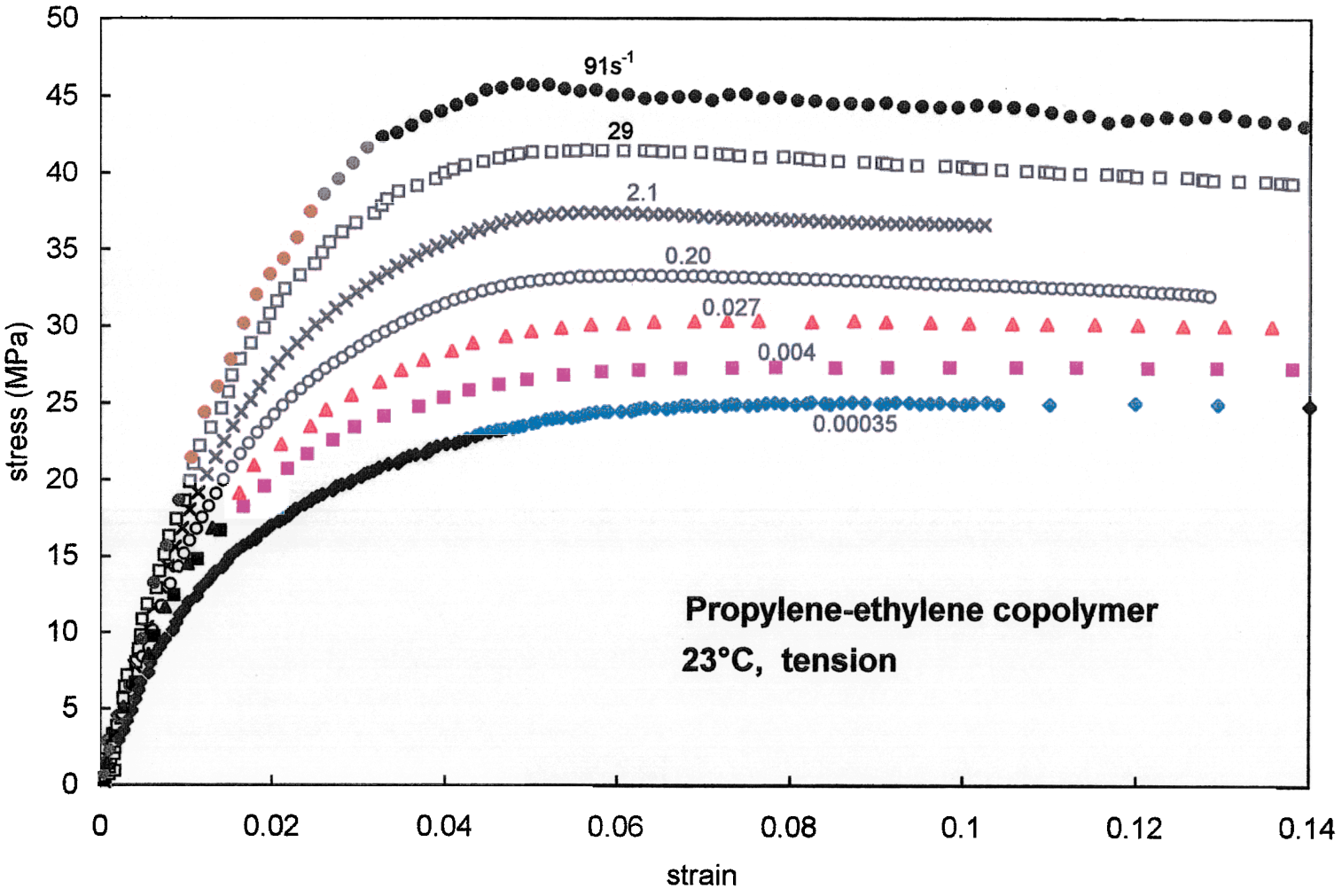
91s-1
29
2.1
0.20
0.027
0.004
0.00035
Propylene-ethylene copolymer
23°C, tension
stress (MPa)
strain
0
5
10
15
20
25
30
35
40
45
50
0
0.02
0.04
0.06
0.08
0.1
0.12
0.14

Fig. 11b

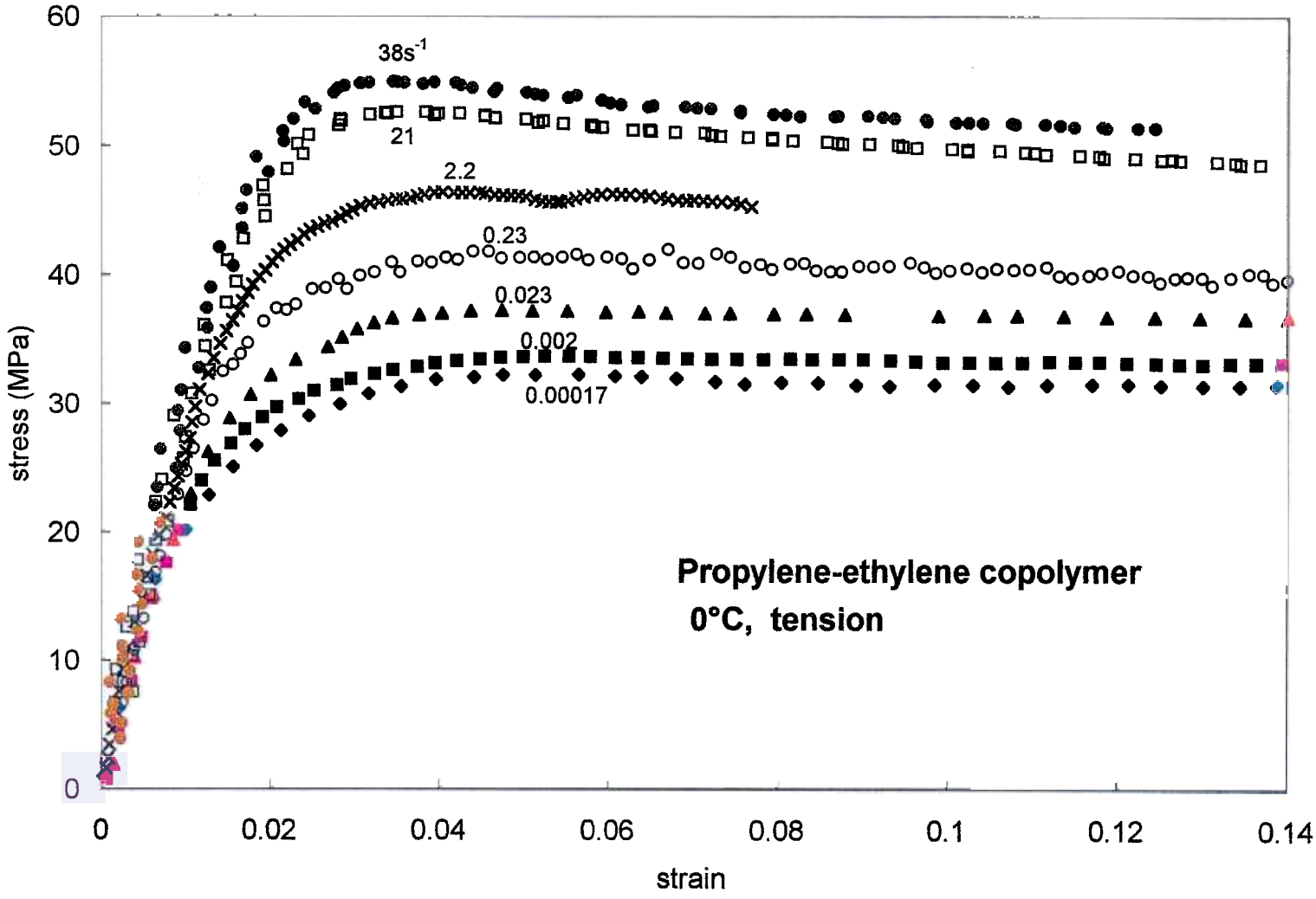
60
50
40
30
20
10
0
stress (MPa)
0
0.02
0.04
0.06
0.08
0.1
0.12
0.14
strain
38s-1
21
2.2
0.23
0.023
0.002
0.00017
Propylene-ethylene copolymer
0°C, tension

Fig. 1c

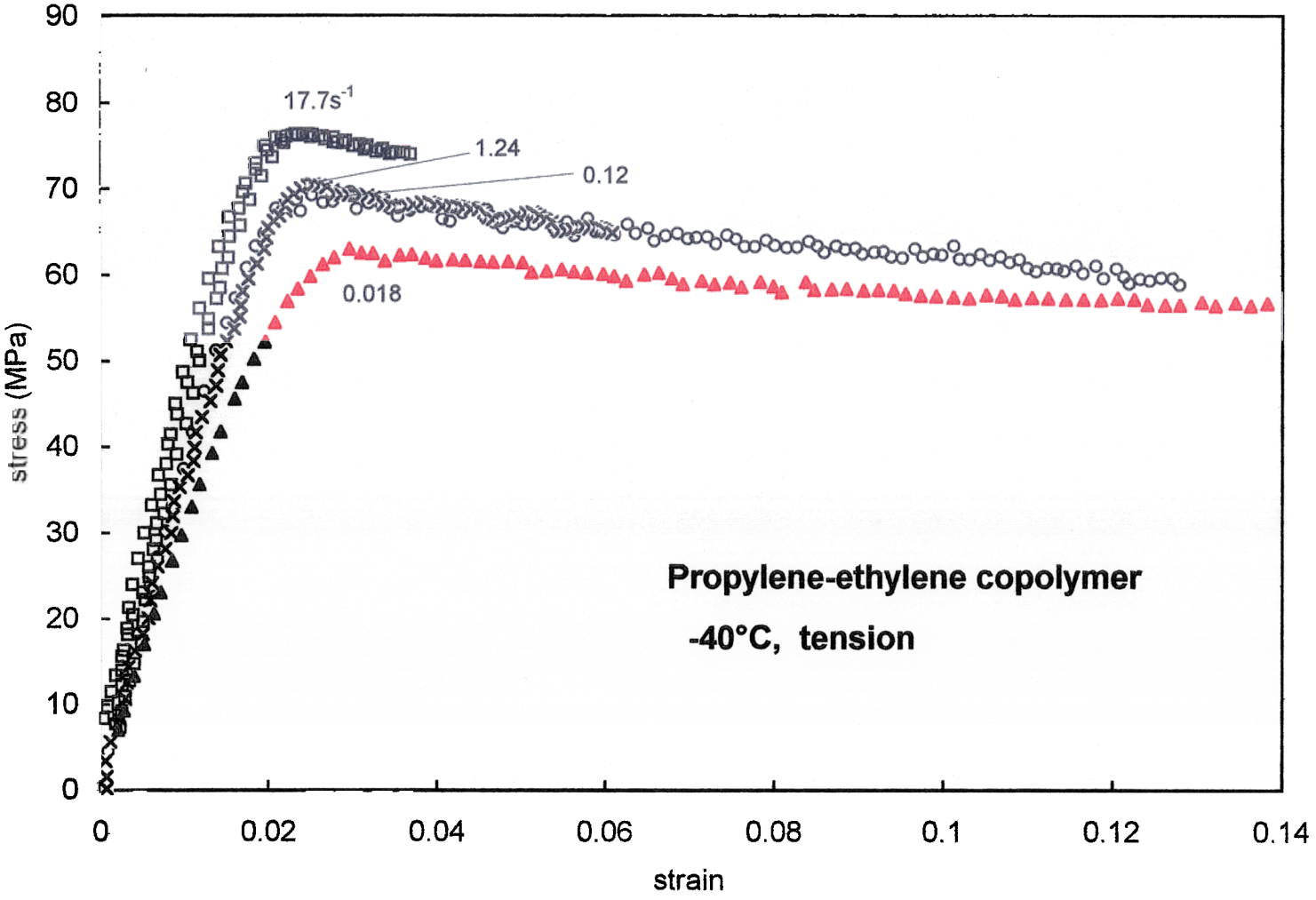
90
80
70
60
50
40
30
20
10
0
stress (MPa)
0
0.02
0.04
0.06
0.08
0.1
0.12
0.14
strain
17.7s-1
1.24
0.12
0.018
Propylene-ethylene copolymer
-40°C, tension

Fig. 11d

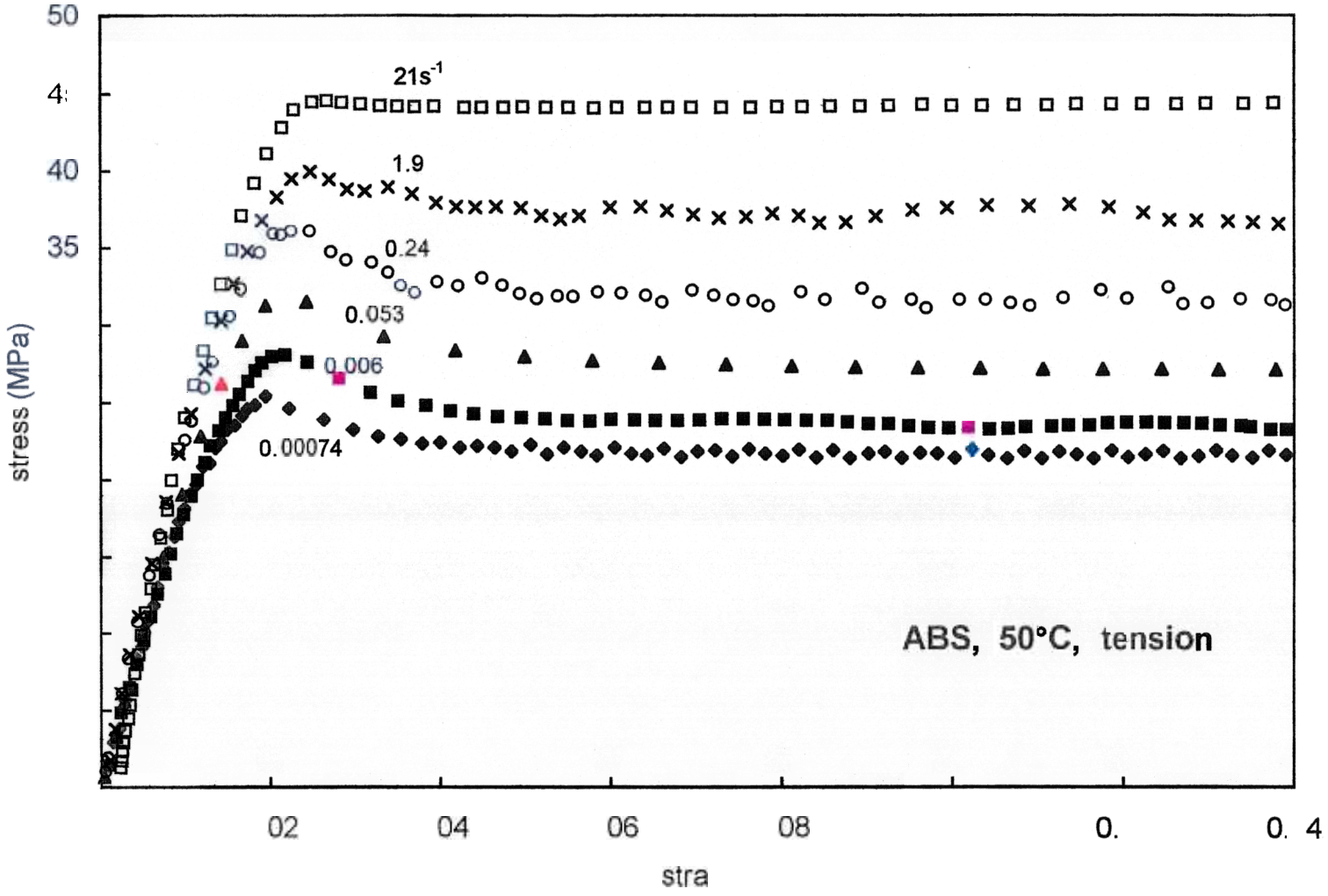
50
40
35
stress (MPa)
21s-1
1.9
0.24
0.053
0.006
0.00074
ABS, 50°C, tension
02
04
06
08
0.
0. 4
stra

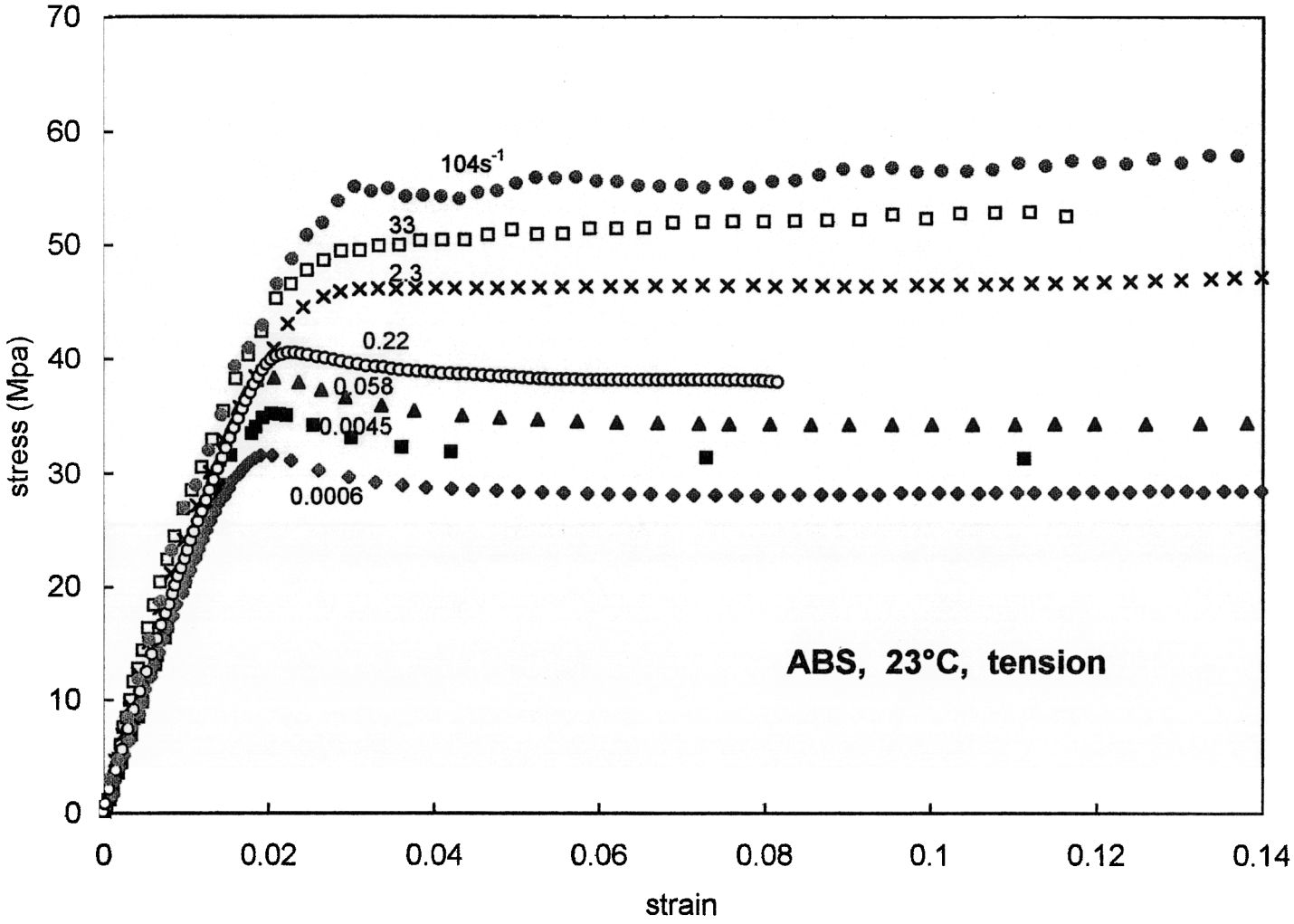
70
60
50
40
30
20
10
0
stress (Mpa)
0
0.02
0.04
0.06
0.08
0.1
0.12
0.14
strain
104s-1
33
2.3
0.22
0.058
0.0045
0.0006
ABS, 23°C, tension

Fig. 12b

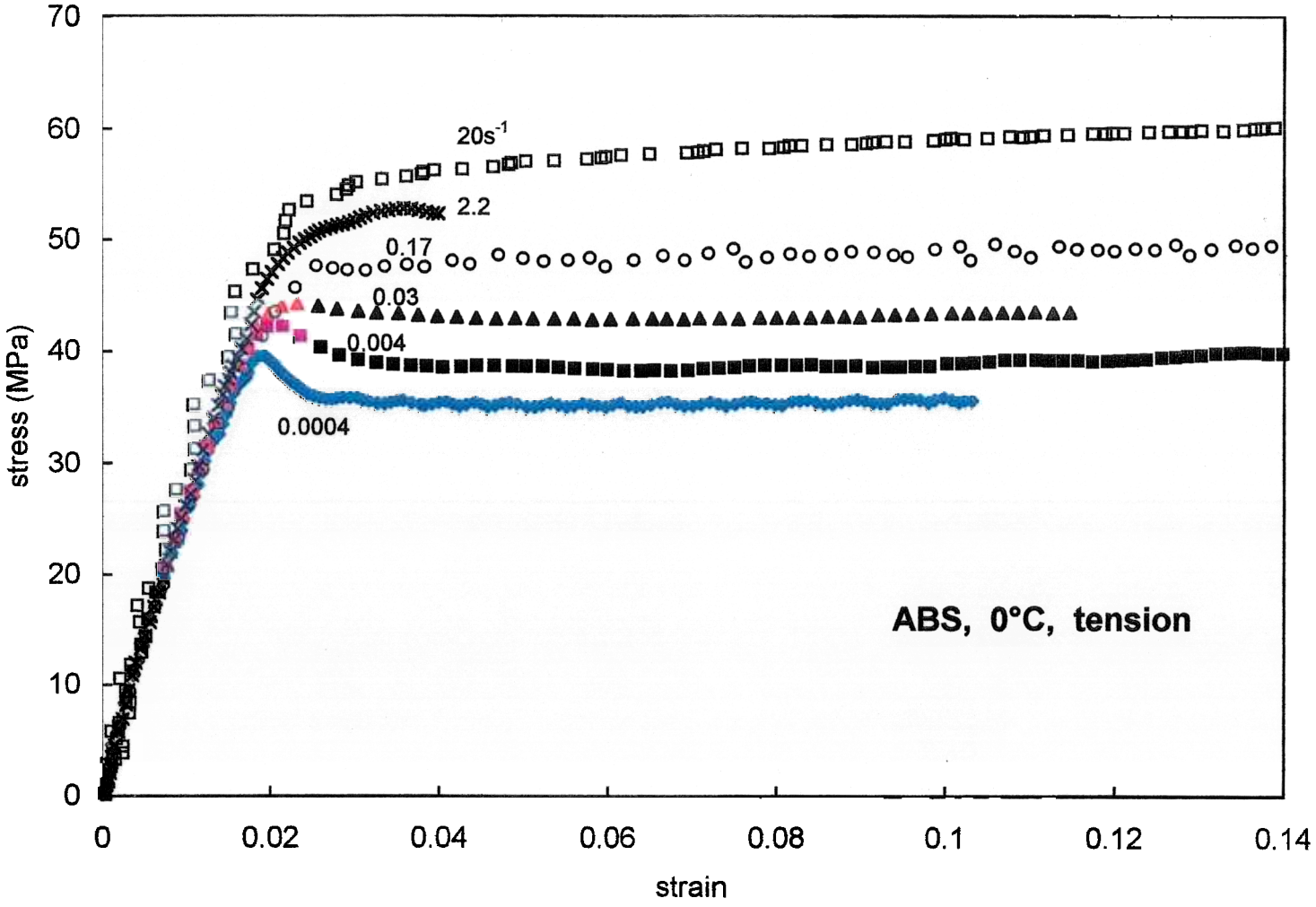
70
60
50
40
30
20
10
0
stress (MPa)
0
0.02
0.04
0.06
0.08
0.1
0.12
0.14
strain
20s-1
2.2
0.17
0.03
0.004
0.0004
ABS, 0°C, tension

Fig. 12c

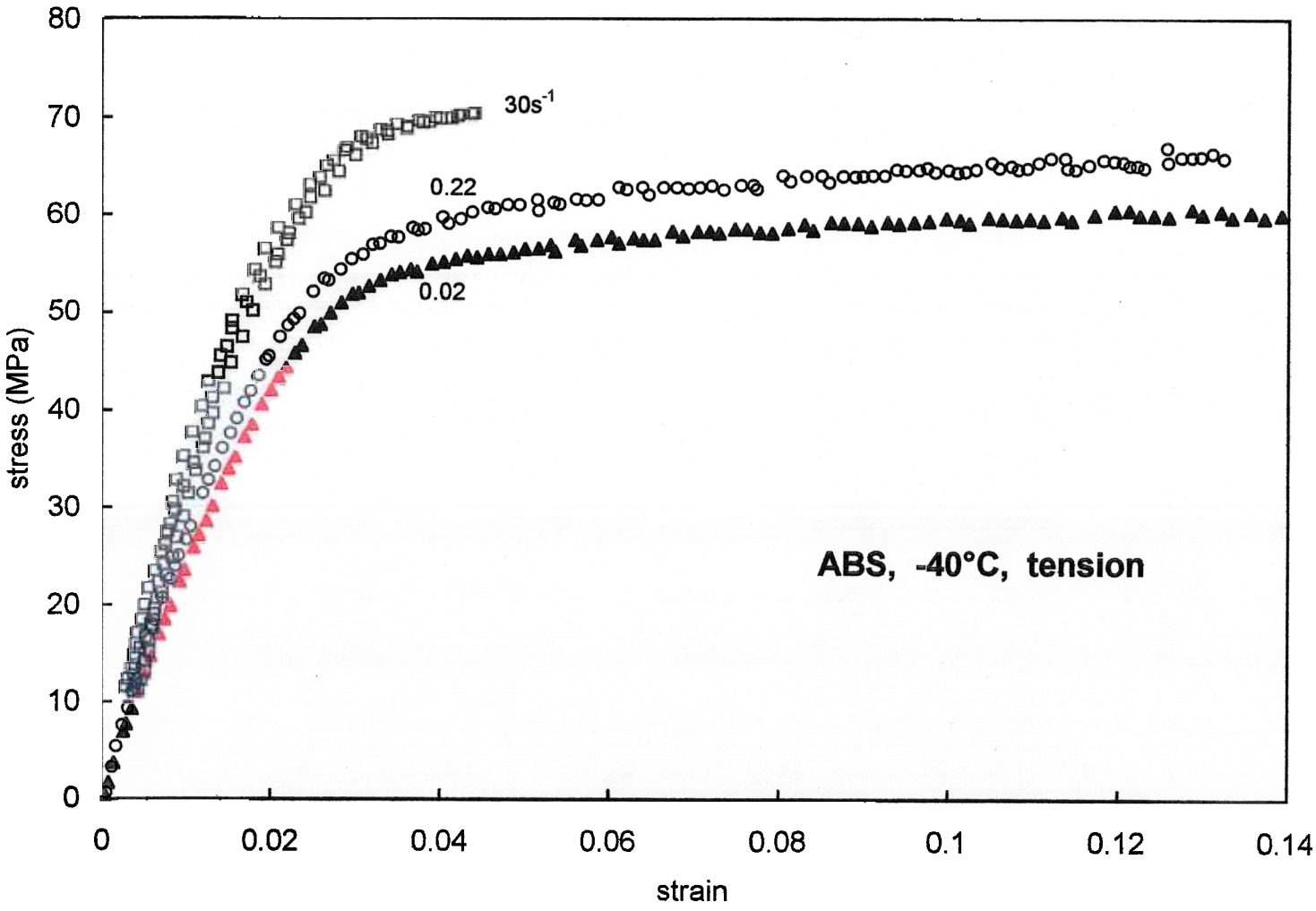
80
70
60
50
40
30
20
10
0
stress (MPa)
0
0.02
0.04
0.06
0.08
0.1
0.12
0.14
strain
30s-1
0.22
0.02
ABS, -40°C, tension

Fig. 12d

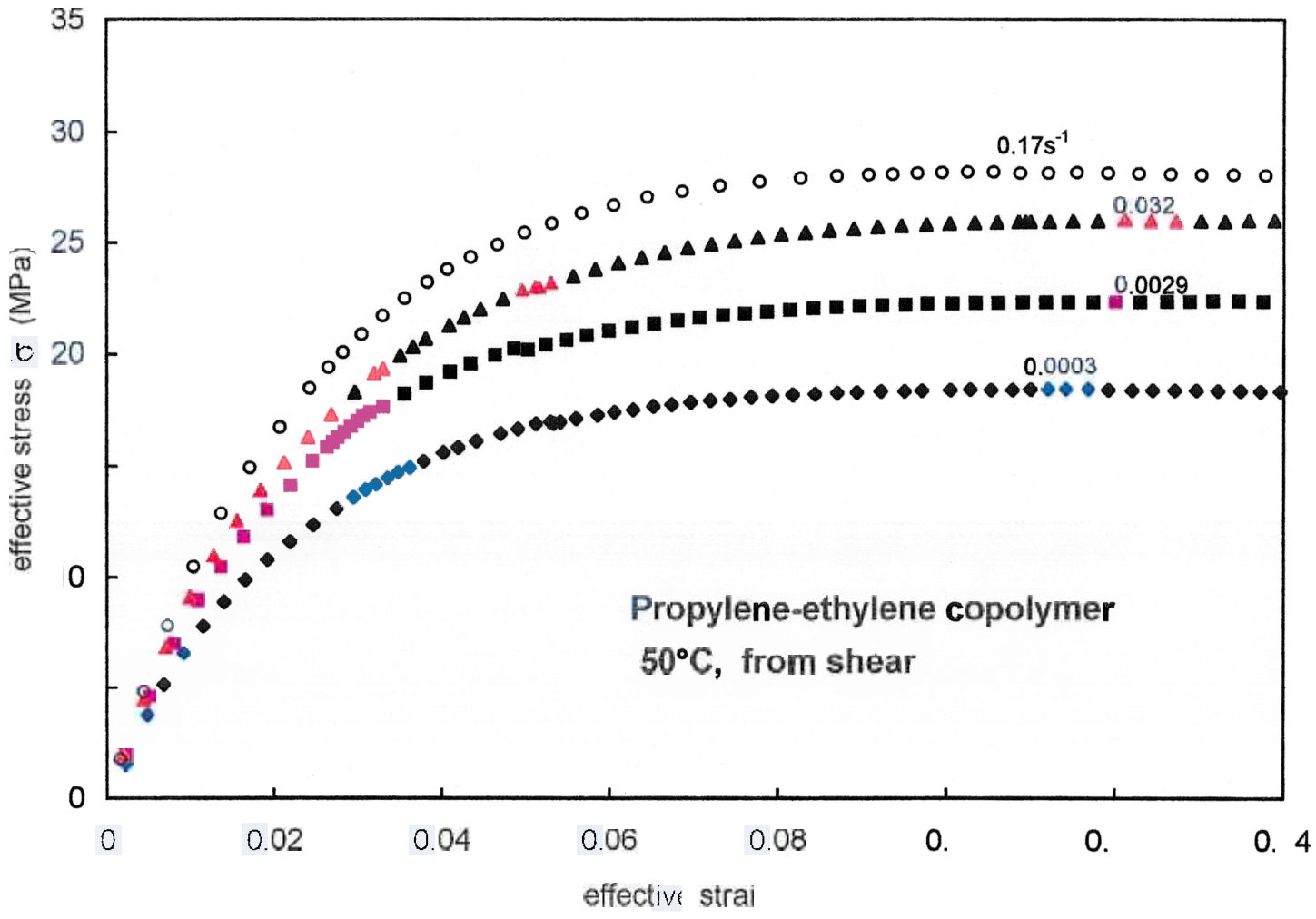
35
30
25
20
0
0
effective stress σ (MPa)
0.17s-1
0.032
0.0029
0.0003
Propylene-ethylene copolymer
50°C, from shear
0
0.02
0.04
0.06
0.08
0.
0.
0. 4
effective strai

Fig 3a

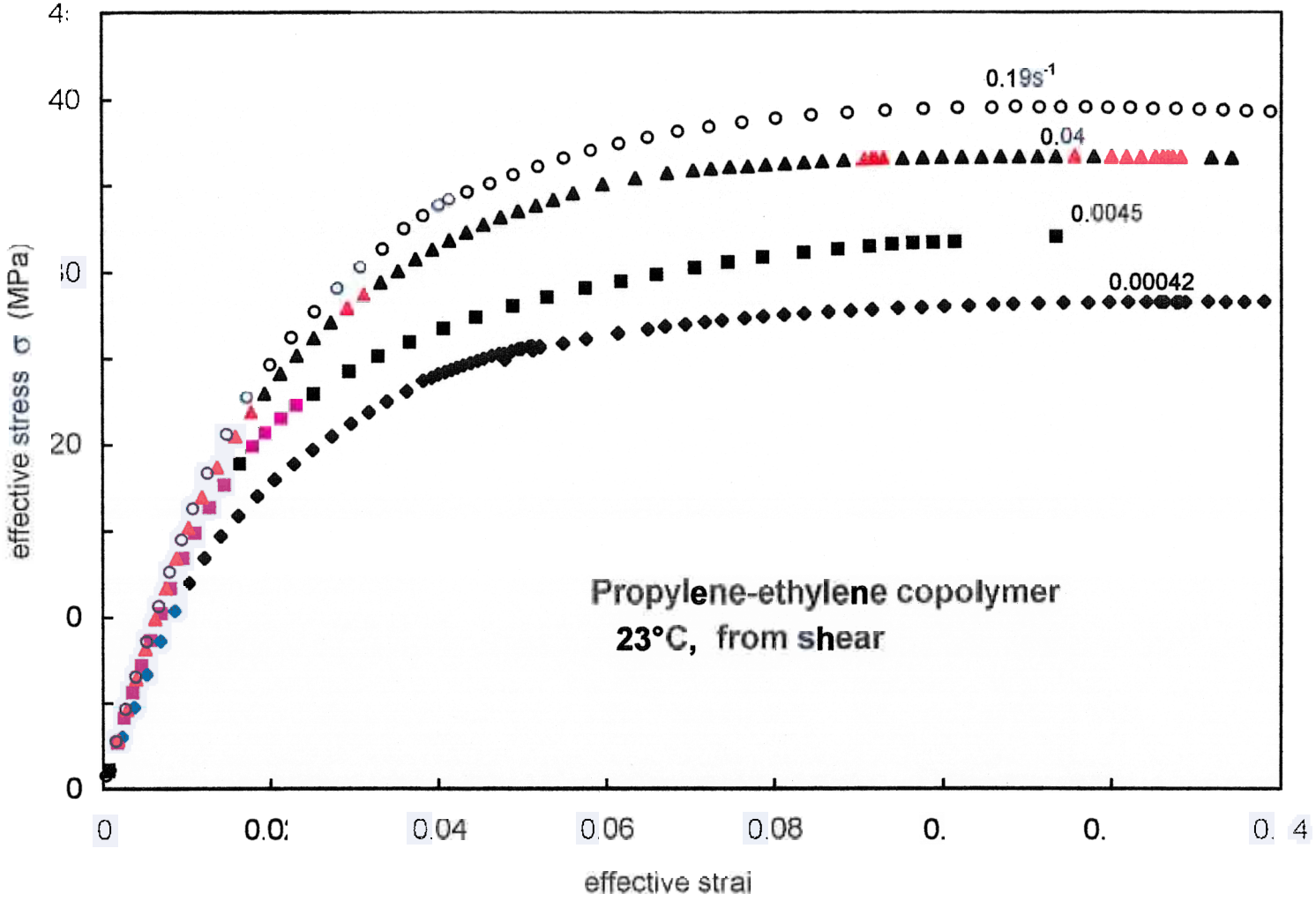
0.19s-1
0.04
0.0045
0.00042
Propylene-ethylene copolymer
23°C, from shear
effective stress σ (MPa)
effective strai
0
20
40
0.04
0.06
0.08

Fig 3b

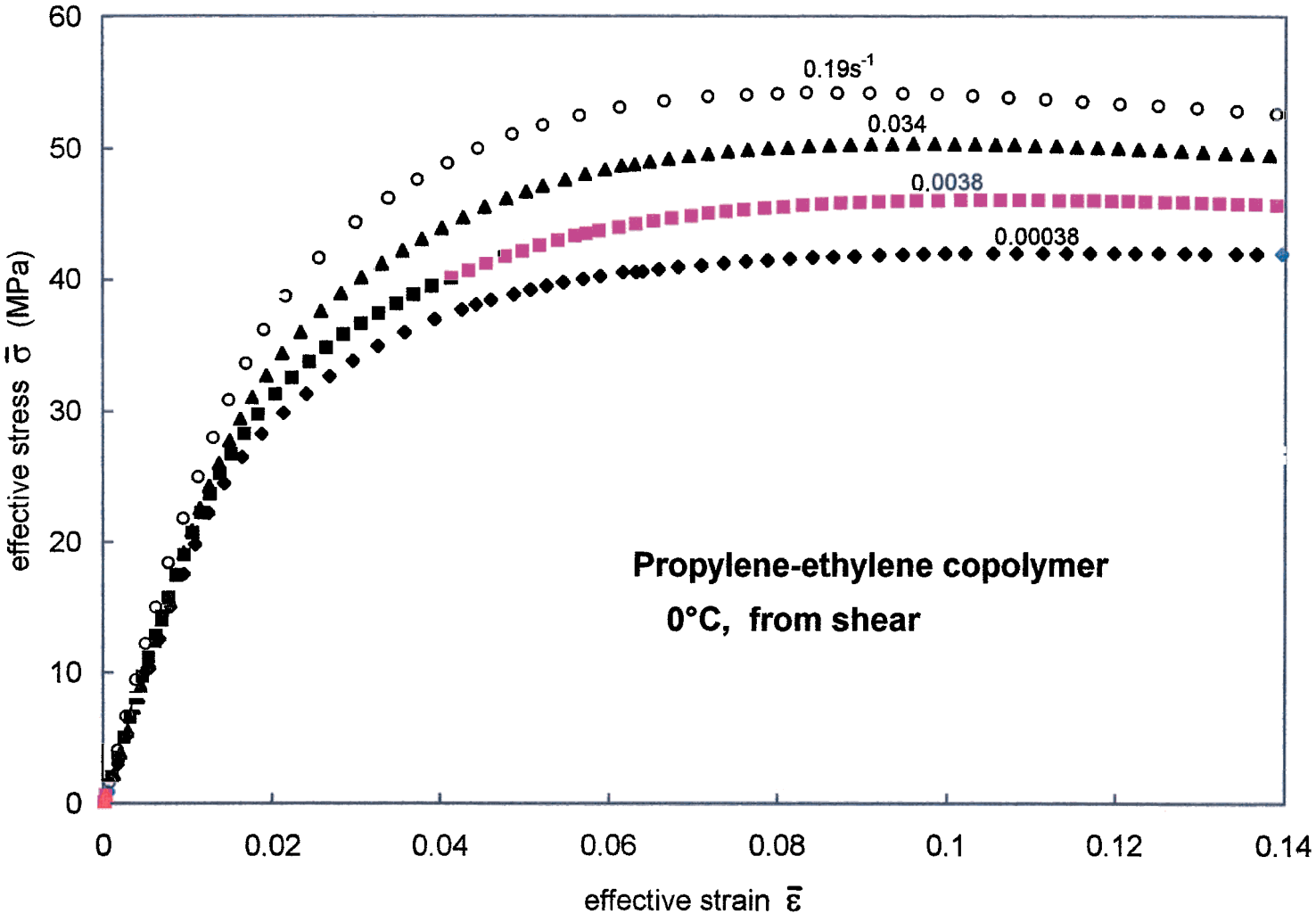
60
50
40
30
20
10
0
0
0.02
0.04
0.06
0.08
0.1
0.12
0.14
effective stress $\bar{\sigma}$ (MPa)
effective strain $\bar{\varepsilon}$
0.19s^{-1}
0.034
0.0038
0.00038
Propylene-ethylene copolymer
0°C, from shear

Fig.13c

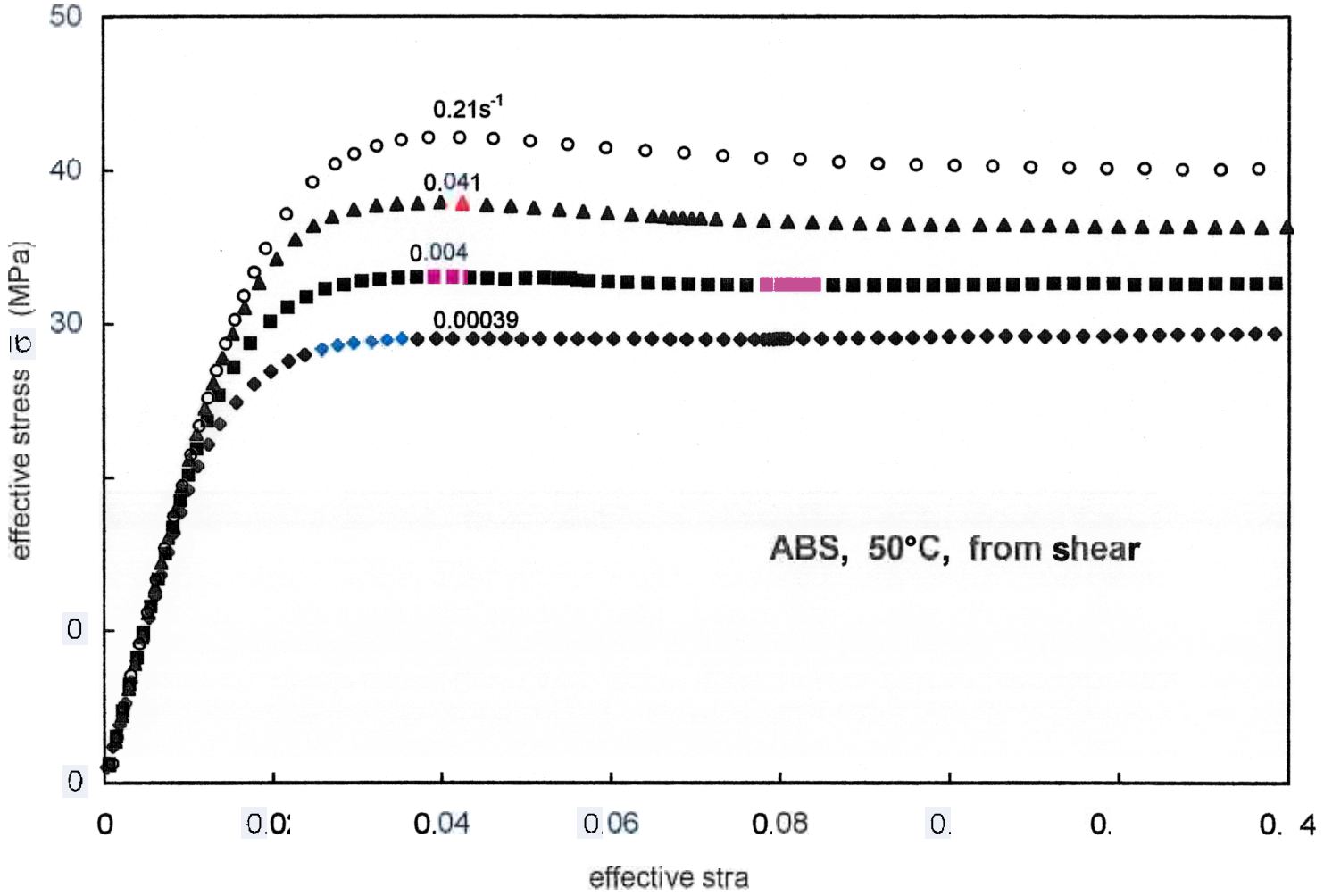
50
40
30
0
0
effective stress σ̄ (MPa)
0.21s-1
0.041
0.004
0.00039
ABS, 50°C, from shear
0
0.0
0.04
0.06
0.08
0.
0.
0. 4
effective stra

Fi 4a

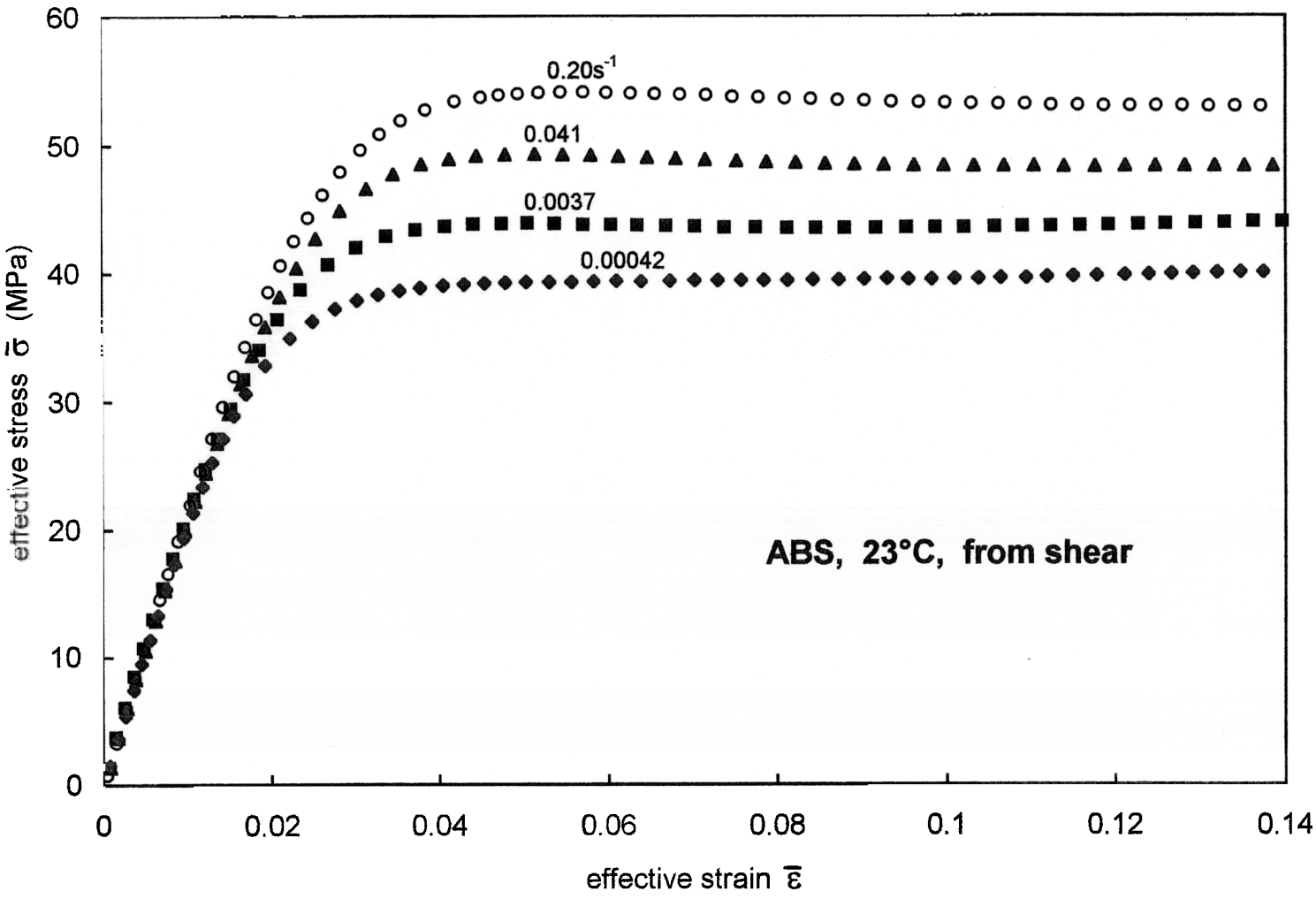
60
50
40
30
20
10
0
0
0.02
0.04
0.06
0.08
0.1
0.12
0.14
effective stress $\bar{\sigma}$ (MPa)
effective strain $\bar{\varepsilon}$
0.20s^{-1}
0.041
0.0037
0.00042
ABS, 23°C, from shear

Fig. 14b

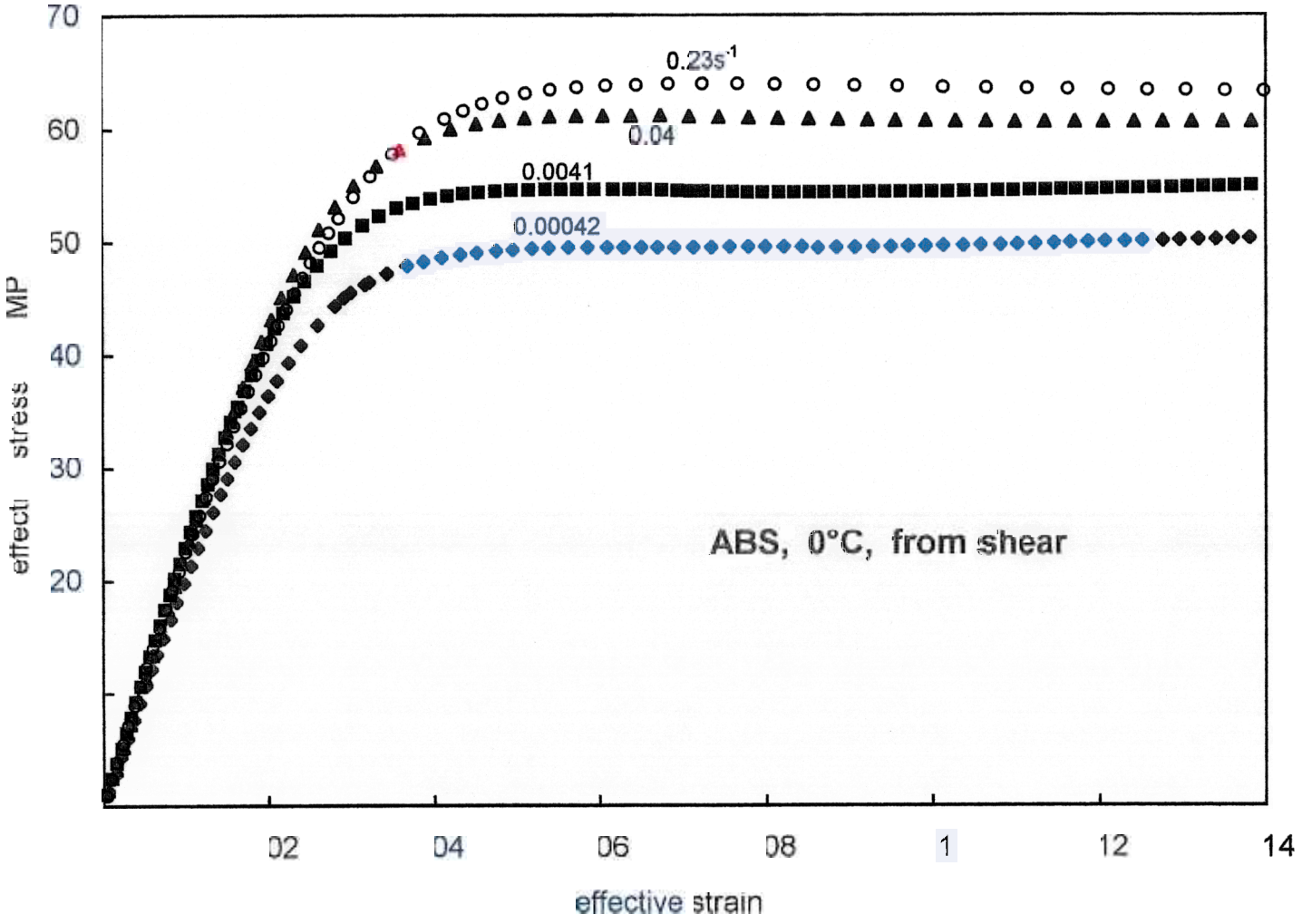
70
60
50
40
30
20
effecti stress MP
0.23s-1
0.04
0.0041
0.00042
ABS, 0°C, from shear
02
04
06
08
1
12
14
effective strain

Fig. 14c

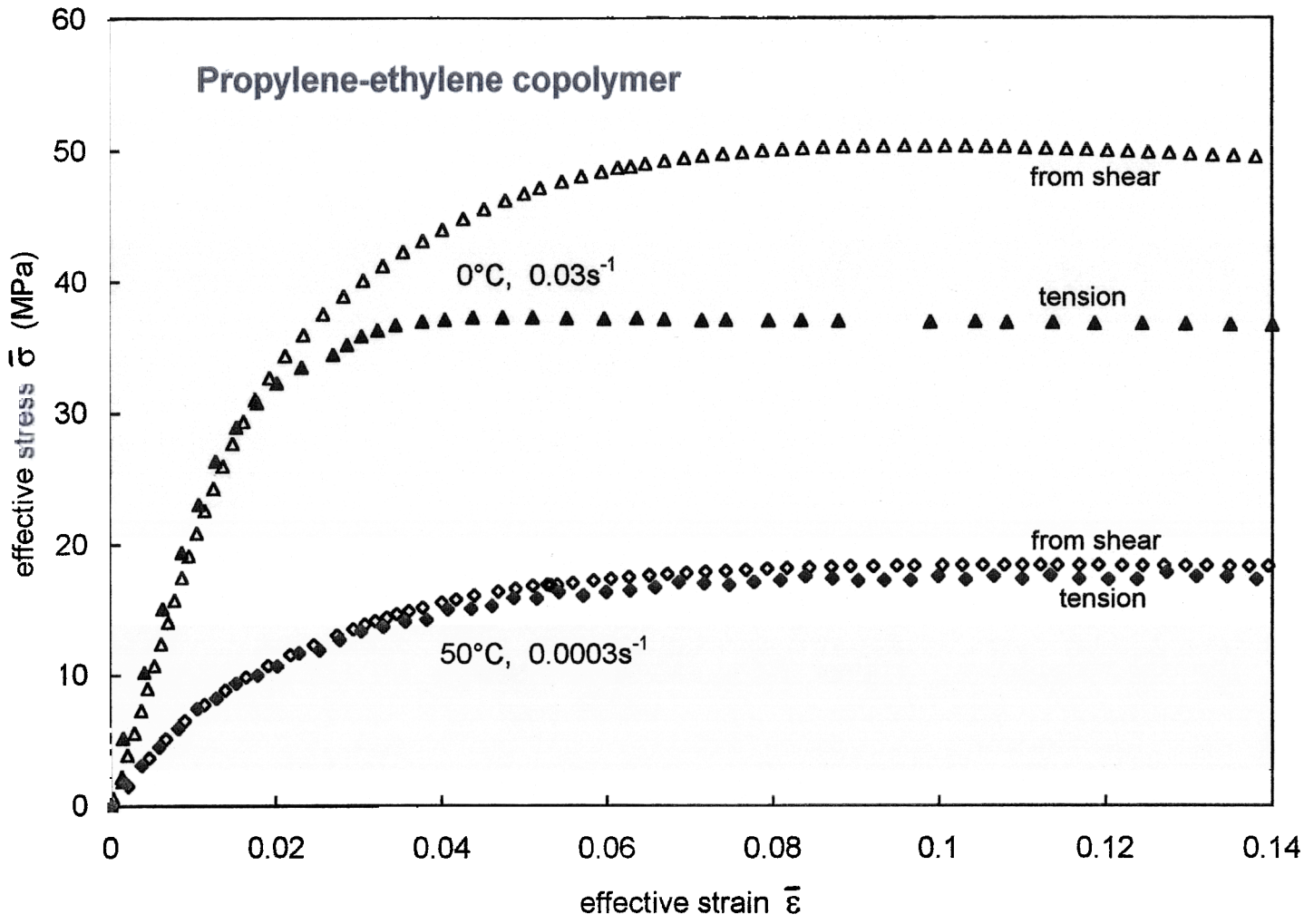
Propylene-ethylene copolymer
from shear
0°C, 0.03s-1
tension
from shear
tension
50°C, 0.0003s-1
effective stress σ̄ (MPa)
effective strain ε̄
0
10
20
30
40
50
60
0
0.02
0.04
0.06
0.08
0.1
0.12
0.14

Fig. 15

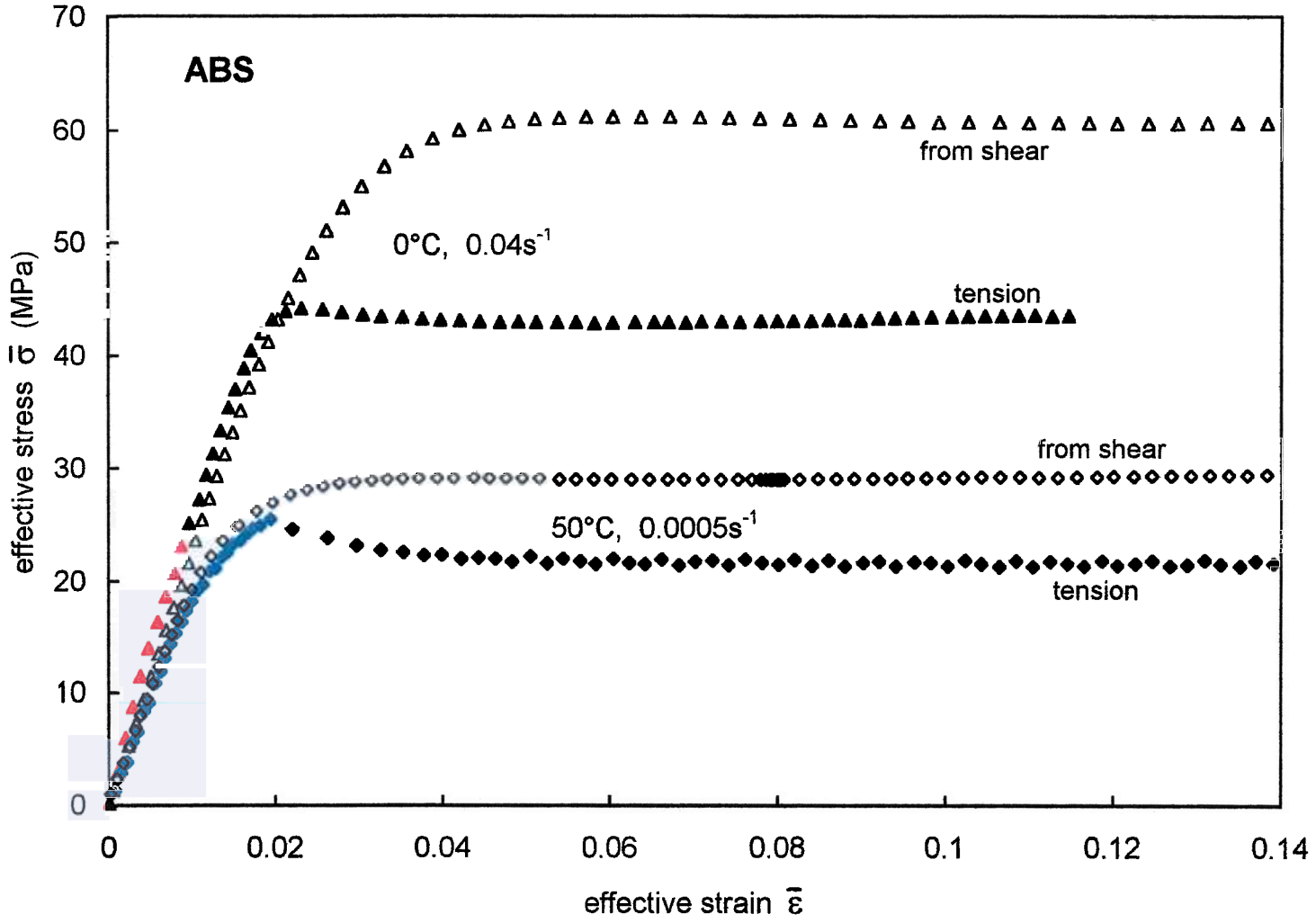
ABS
70
60
50
40
30
20
10
0
effective stress $\bar{\sigma}$ (MPa)
from shear
0°C, 0.04s^{-1}
tension
from shear
50°C, 0.0005s^{-1}
tension
0
0.02
0.04
0.06
0.08
0.1
0.12
0.14
effective strain $\bar{\varepsilon}$

Fig. 16

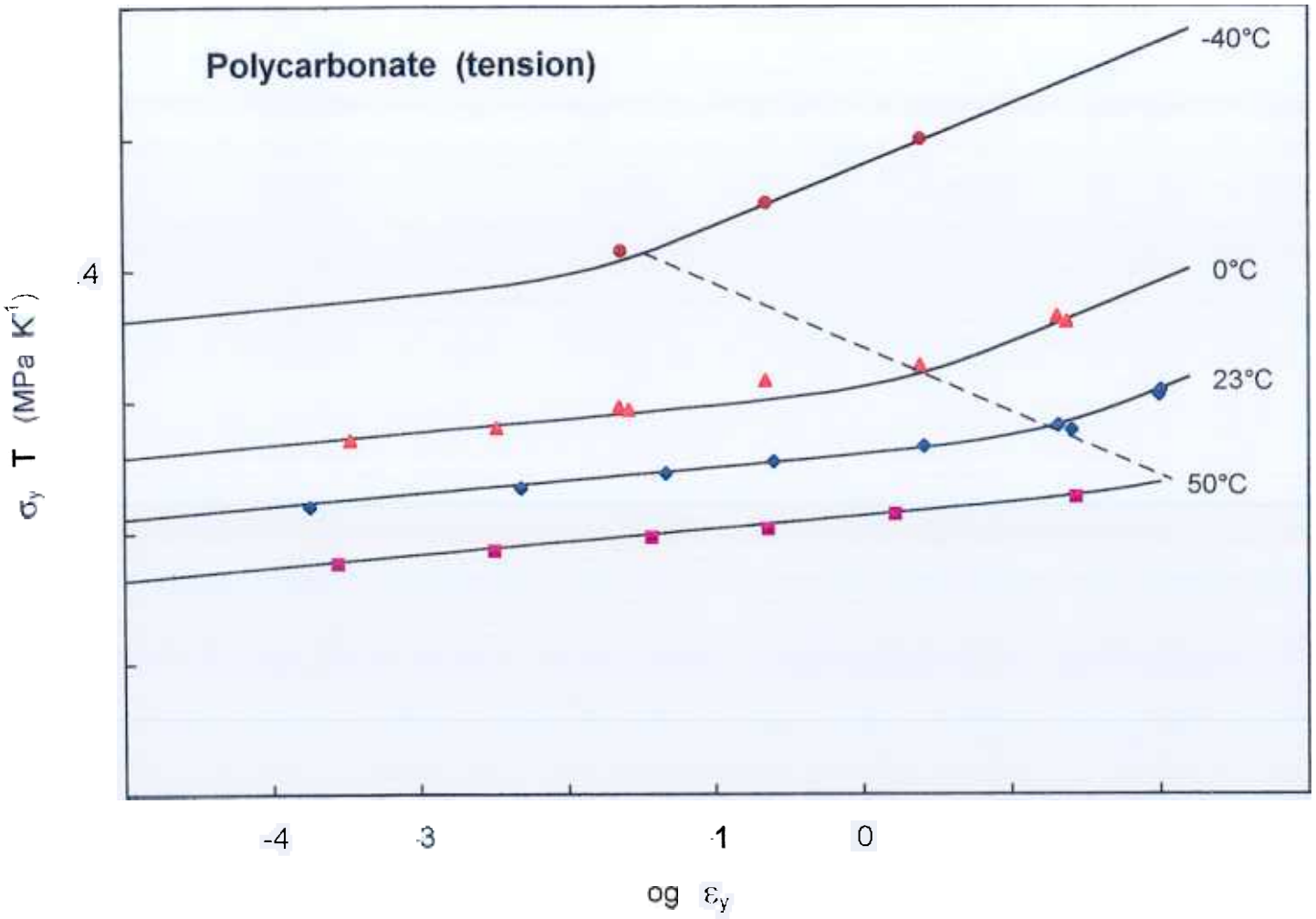
Polycarbonate (tension)
-40°C
0°C
23°C
50°C
.4
-4
-3
-1
0
σ_y T (MPa K^{-1})
og ε_y

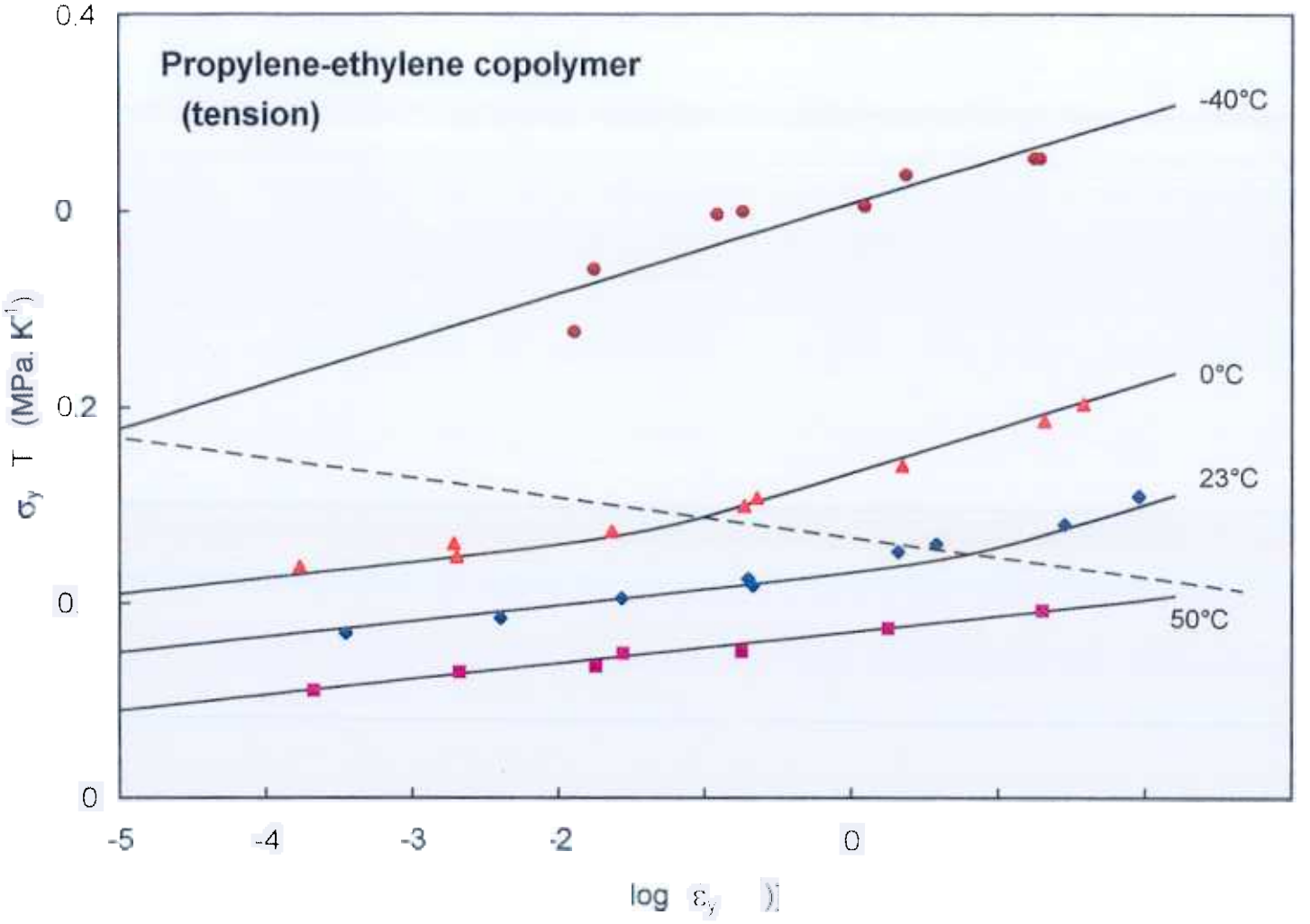
Propylene-ethylene copolymer
(tension)
-40°C
0°C
23°C
50°C
0.4
0
0.2
0
0
-5
-4
-3
-2
0
σy T (MPa. K-1)
log εy)

Fig. 8

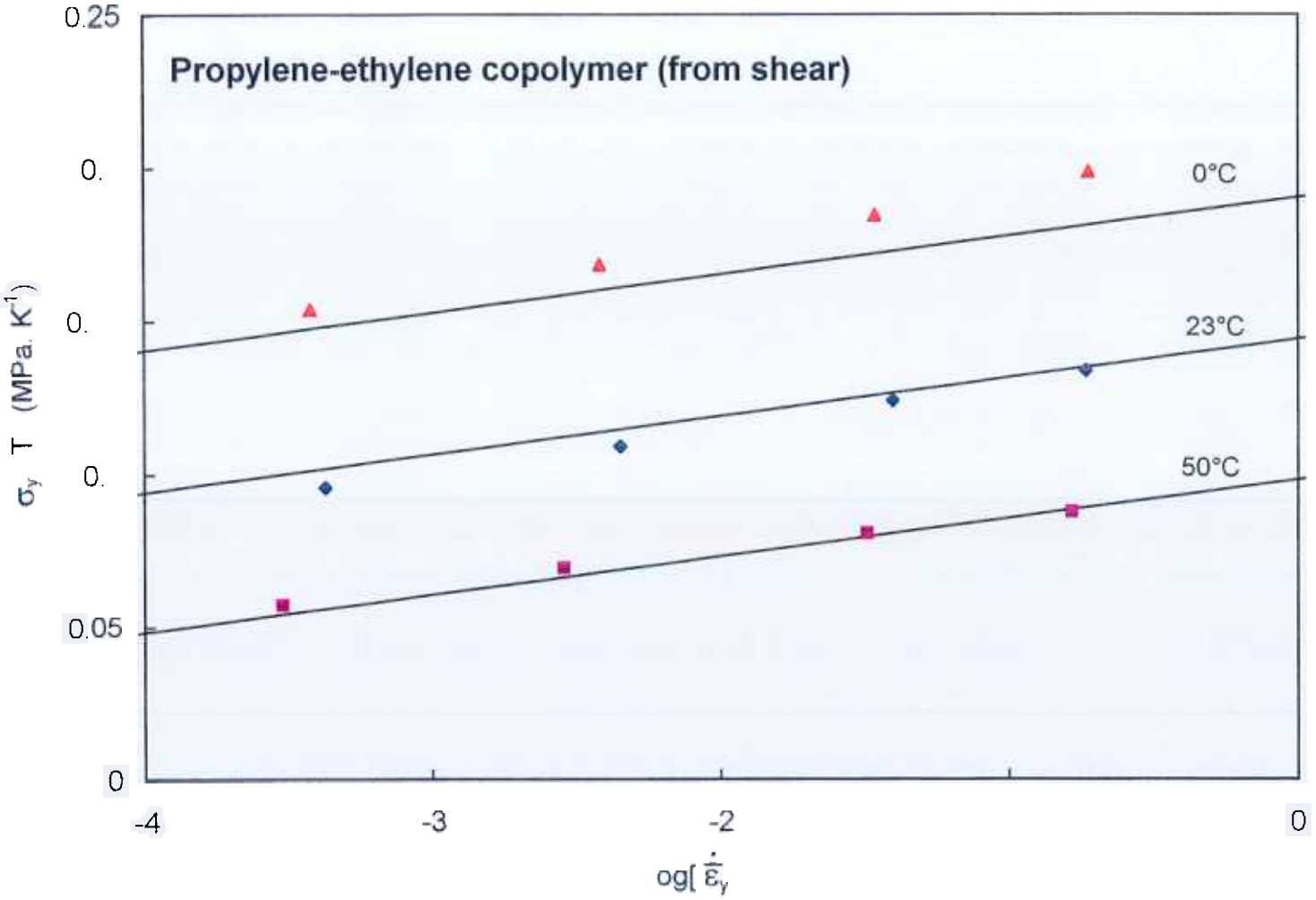
Propylene-ethylene copolymer (from shear)
0.25
0.
0.
0.
0.05
0
0°C
23°C
50°C
-4
-3
-2
0
σ_y T (MPa. K^{-1})
og[$\dot{\varepsilon}_y$

Fig.

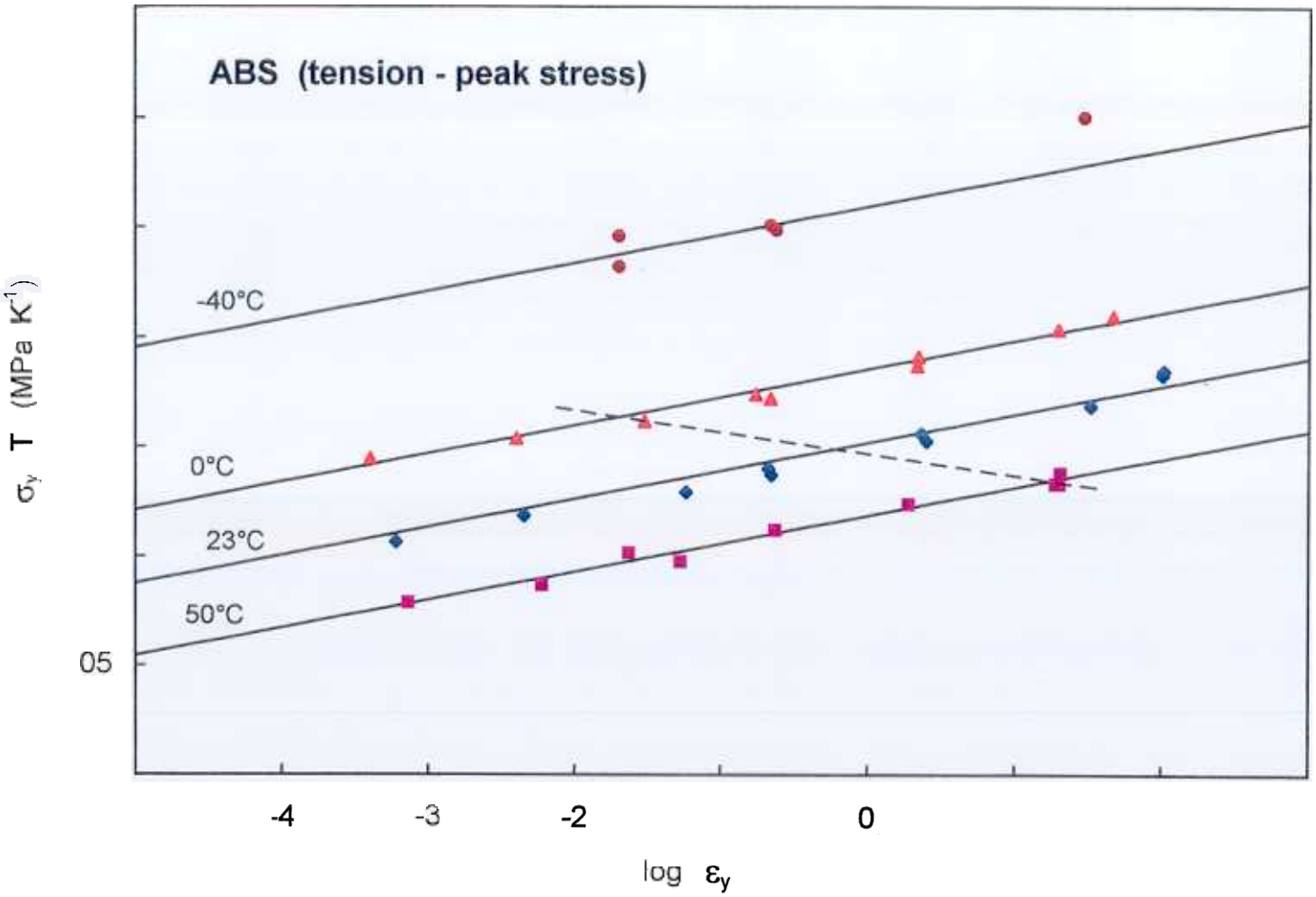
ABS (tension - peak stress)
-40°C
0°C
23°C
50°C
05
-4
-3
-2
0
log εy
σy T (MPa K-1)

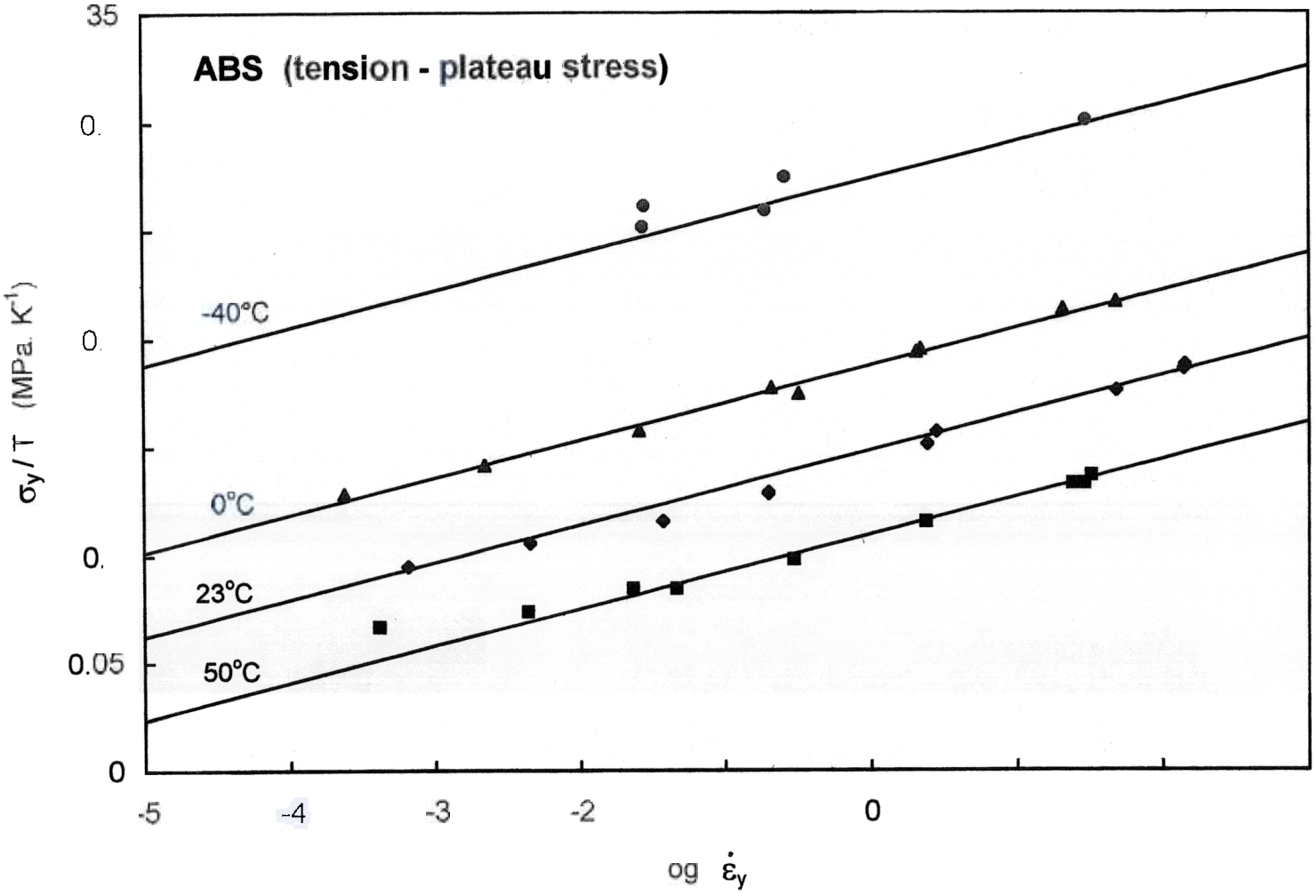
ABS (tension - plateau stress)
35
0.
0
0.
0.05
0
-40°C
0°C
23°C
50°C
σy / T (MPa. K-1)
-5
-4
-3
-2
0
og ε̇y

Fig

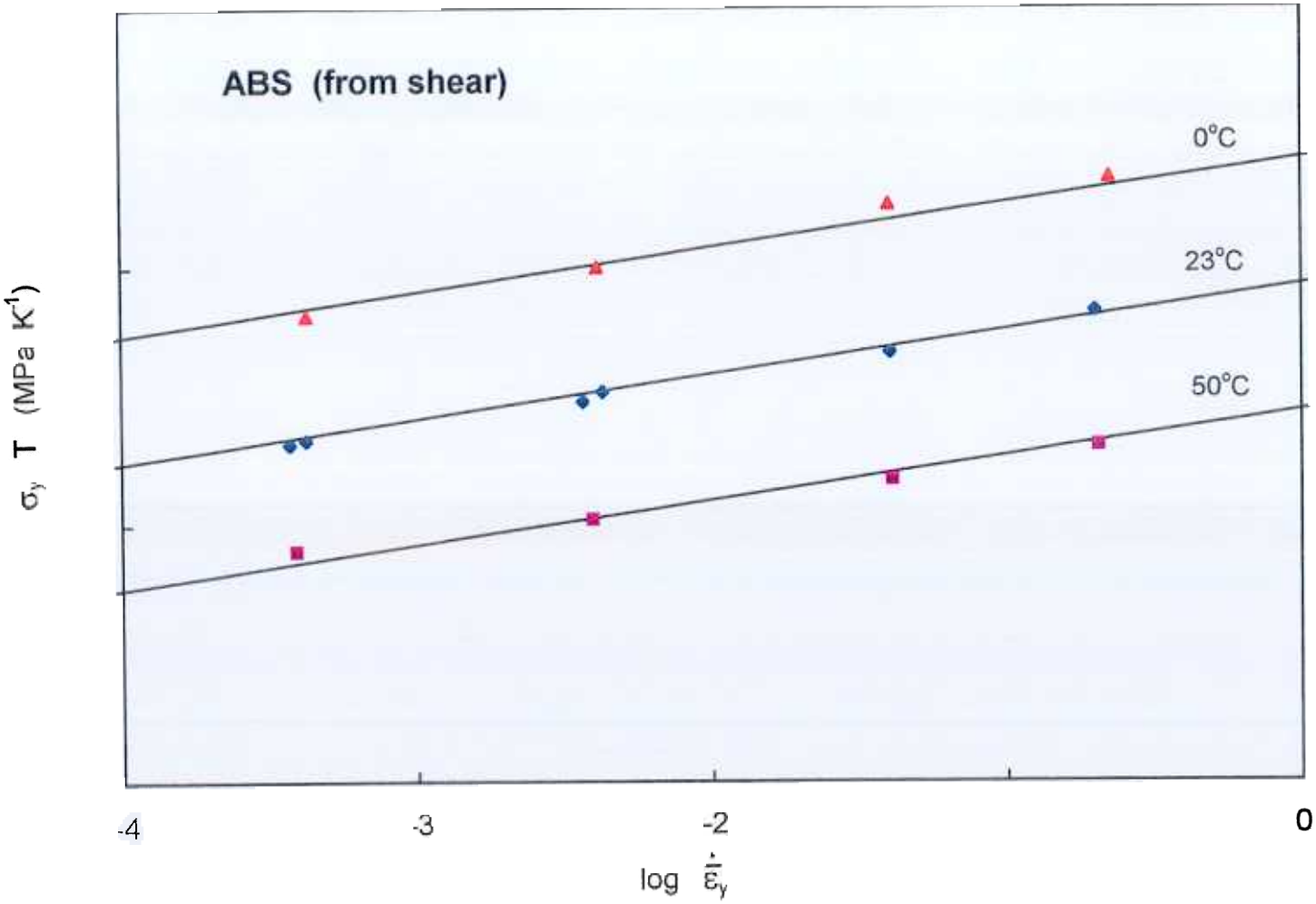
ABS (from shear)
0°C
23°C
50°C
σ_y T (MPa K^{-1})
-4
-3
-2
0
log $\dot{\varepsilon}_y$

Fig. 22